Available online at www.sciencedirect.com

ScienceDirect

Geochimica et Cosmochimica Acta 222 (2018) 230–252

Geochimica et Cosmochimica Acta

www.elsevier.com/locate/gca

Low-temperature aqueous alteration on the CR chondrite parent body: Implications from *in situ* oxygen-isotope analyses

Christine E. Jilly-Rehak [a,b,*], Gary R. Huss [b], Kazu Nagashima [b], Devin L. Schrader [c]

[a] *Department of Geology & Geophysics, University of Hawai'i at Mānoa, 1680 East-West Rd. POST 517A, Honolulu, HI 96822, USA*
[b] *Hawai'i Institute of Geophysics and Planetology, University of Hawai'i at Mānoa, 1680 East-West Rd. POST 602, Honolulu, HI 96822, USA*
[c] *Center for Meteorite Studies, School of Earth and Space Exploration, Arizona State University, PO Box 871404, Tempe, AZ 85287, USA*

Received 17 March 2017; accepted in revised form 4 October 2017; Available online 19 October 2017

Abstract

The presence of hydrated minerals in chondrites indicates that water played an important role in the geologic evolution of the early Solar System; however, the process of aqueous alteration is still poorly understood. Renazzo-like carbonaceous (CR) chondrites are particularly well-suited for the study of aqueous alteration. Samples range from being nearly anhydrous to fully altered, essentially representing snapshots of the alteration process through time. We studied oxygen isotopes in secondary-minerals from six CR chondrites of varying hydration states to determine how aqueous fluid conditions (including composition and temperature) evolved on the parent body. Secondary minerals analyzed included calcite, dolomite, and magnetite. The O-isotope composition of calcites ranged from $\delta^{18}O \approx 9$ to 35‰, dolomites from $\delta^{18}O \approx 23$ to 27‰, and magnetites from $\delta^{18}O \approx -18$ to 5‰. Calcite in less-altered samples showed more evidence of fluid evolution compared to heavily altered samples, likely reflecting lower water/rock ratios. Most magnetite plotted on a single trend, with the exception of grains from the extensively hydrated chondrite MIL 090292. The MIL 090292 magnetite diverges from this trend, possibly indicating an anomalous origin for the meteorite. If magnetite and calcite formed in equilibrium, then the relative ^{18}O fractionation between them can be used to extract the temperature of co-precipitation. Isotopic fractionation in Al Rais carbonate-magnetite assemblages revealed low precipitation temperatures (~60 °C). Assuming that the CR parent body experienced closed-system alteration, a similar exercise for parallel calcite and magnetite O-isotope arrays yields "global" alteration temperatures of ~55 to 88 °C. These secondary mineral arrays indicate that the O-isotopic composition of the altering fluid evolved upon progressive alteration, beginning near the Al Rais water composition of $\Delta^{17}O \sim 1$‰ and $\delta^{18}O \sim 10$‰, and becoming increasingly ^{16}O-enriched toward a final fluid composition of $\Delta^{17}O \sim -1.2$‰ and $\delta^{18}O \sim -15$‰.

Keywords: CR chondrite; Carbonaceous chondrites; Aqueous alteration; Secondary processes; Oxygen isotopes

1. INTRODUCTION

The Renazzo-like carbonaceous (CR) chondrites record the process of parent-body aqueous alteration better than any other chondrite group. CR chondrites range from almost completely altered to nearly anhydrous, while experiencing only minor degrees of thermal metamorphism (e.g., Weisberg et al., 1993, 1995; Kallemeyn et al., 1994; Krot et al., 2002; Brearley, 2006; Rubin et al., 2007; Weisberg and Huber, 2007; Schrader et al., 2011, 2015; Harju et al., 2014). Most aqueous-alteration literature is dominated by studies of Mighei-like (CM) and Ivuna-like (CI) chondrites, since they have experienced extensive aqueous alteration (e.g., Rubin et al., 2007). Yet unlike for the

* Corresponding author at: Space Sciences Lab, University of California, Berkeley, 7 Gauss Way, Berkeley, CA 94720, USA.
E-mail addresses: jillyrehak@ssl.berkeley.edu (C.E. Jilly-Rehak), ghuss@higp.hawaii.edu (G.R. Huss), kazu@higp.hawaii.edu (K. Nagashima), devin.schrader@asu.edu (D.L. Schrader).

https://doi.org/10.1016/j.gca.2017.10.007
0016-7037/

CR chondrites, the inferred mineralogy of the precursor CM and CI material is based upon many assumptions due to the relative lack of unaltered components. Other chondrite groups, such as Vigarano-like (CV), Ornans-like (CO) and Ordinary (OC) chondrites, have undergone minor amounts of aqueous alteration, but have also experienced extensive thermal metamorphism that can obscure and complicate aqueous alteration signatures (e.g., Brearley, 2006; Weisberg et al., 2006).

CR chondrites are characterized by large (~0.7 mm) metal-rich type-I chondrules. The type-I chondrules typically consist of olivine and/or pyroxene phenocrysts and abundant Fe,Ni metal nodules set within a glassy or microcrystalline mesostasis. Some chondrules are more complex and exhibit a multi-layered structure, with the outer layers consisting of smaller pyroxene-rich grains (Weisberg et al., 1993; Kallemeyn et al., 1994; Weisberg et al., 2006). The majority of Fe,Ni sulfide phases (troilite, pyrrhotite, and pentlandite) are primary and are associated with type-II chondrules (Schrader et al., 2015), although some instances of secondary sulfides do occur in heavily altered samples. The degree of aqueous alteration varies between samples, and sometimes even between clasts in a single sample. In more aqueously altered lithologies, metal has been oxidized to magnetite, and chondrule mesostasis and silicates have been altered to phyllosilicates (including serpentine, chlorite, and smectite) and carbonates in some cases (e.g., Jilly-Rehak et al., 2017). Fine-grained rim assemblages of phyllosilicates, carbonates, sulfides, and iron oxides occur around some heavily altered chondrules. CRs consist of ~30 to 60% matrix material, including fine-grained dark inclusions that exist as lithic clasts in the host meteorite (Weisberg et al., 1993; Kallemeyn et al., 1994; Weisberg et al., 2006; Schrader et al., 2011). The matrix is primarily comprised of hydrous, anhydrous, and amorphous silicates in quantities that depend on the degree of alteration (Weisberg et al., 1993; Brearley, 2006; Abreu and Brearley, 2010; Howard et al., 2015). Fine-grained carbonates, sulfides, and magnetite are also littered throughout the matrix. The dark inclusions are more hydrated than the interchondrule matrix, but are otherwise petrographically and compositionally very similar. Such dark inclusions typically contain small chondrules (<200 μm), as does the matrix (Weisberg et al., 1993).

The extreme heterogeneity in CR samples has led to difficulties in establishing a consistent petrologic-type classification that describes the relative alteration states of the samples (Weisberg et al., 1993; Weisberg and Huber, 2007; Abreu and Brearley, 2010; Schrader et al., 2011, 2014a; Alexander et al., 2013; Harju et al., 2014; Abreu, 2015, 2016; Howard et al., 2015). Numerous schemes have been proposed, based on various parameters such as whole-rock O-isotope composition, petrography, mineralogy, and H abundance (Alexander et al., 2013; Harju et al., 2014; Schrader et al., 2014a; Abreu, 2015, 2016; Howard et al., 2015). All schemes designate the heavily altered samples as type CR1, and the least altered samples as type CR3, with the exception of the system proposed by Harju et al. (2014), which labels the highly altered samples as CR2.0 instead of CR1. While some overall alteration trends are consistent among the proposed sequences, no scheme can fully account for the complex variations in clast, component, and dark-inclusion abundances across the CR spectrum. For the purpose of this O-isotope paper, we will refer to the degree of alteration roughly quantified by Harju et al. (2014), which correlates with bulk O isotopes (Choi et al., 2009; Schrader et al., 2011; Harju et al., 2014).

In situ O-isotope analyses of secondary (i.e., aqueously-formed) phases are crucial to understanding the aqueous alteration process. On an O three-isotope plot depicting $^{18}O/^{16}O$ vs. $^{17}O/^{16}O$, bulk samples and constituents of CR chondrites plot along a unique two-component mixing line of slope ~0.7 between the terrestrial fractionation line (TFL) and the carbonaceous chondrite anhydrous mineral line (CCAM) (e.g., Clayton and Mayeda, 1999; Choi et al., 2009; Schrader et al., 2011, 2014a). This mixing line reflects the progressive alteration of an ^{16}O-rich anhydrous reservoir by a more $^{17,18}O$-rich H_2O reservoir (Clayton and Mayeda, 1999; Schrader et al., 2011). The anhydrous reservoir is composed of primitive components that lie on the CCAM and/or the primitive chondrule mineral line (PCM; Ushikubo et al., 2012), such as chondrules and calcium-aluminum inclusions (CAIs) (e.g., Krot et al., 2006; Weisberg et al., 2006; Makide et al., 2009; Ushikubo et al., 2012; Schrader et al., 2013, 2014b; Tenner et al., 2015). Anhydrous chondrule silicates in CR chondrites have negative $\Delta^{17}O$ compositions relative to the TFL, with the exception of type-II chondrules, which are rare in CRs (Connolly and Huss, 2010; Schrader et al., 2013; 2014b, 2017; Tenner et al., 2015). The heavy O reservoir is thought to be the source of the altering fluid on the CR parent body, but may not represent the same heavy O reservoir responsible for the hydration of CI and CM chondrites (Clayton and Mayeda, 1984, 1999; Weisberg et al., 1995; Schrader et al., 2011). While the whole-rock mixing line serves as a broad generalization for progressive alteration, there are fine scale inconsistencies where the alteration states of some specimens do not perfectly correlate with their anticipated composition (Schrader et al., 2011, 2014a). Such inconsistencies likely reflect the extreme heterogeneity of components in CR chondrites (Weisberg et al., 1993). *In situ* O-isotope analyses of individual phases are needed to define the secondary-mineral contributions to the bulk CR trend.

Oxygen isotopic compositions of secondary minerals can also be used to constrain the temperatures of aqueous alteration on the CR parent body (e.g., Chiba et al., 1989; Zheng, 1998; Choi et al., 2000). During secondary-mineral precipitation, O isotopes are fractionated between the water and the mineral phases. The degree of fractionation is highly dependent on temperature and has been determined empirically for a variety of secondary minerals (including calcite, dolomite, and magnetite) under terrestrial conditions (e.g., Chiba et al., 1989; Zheng, 1991, 1995, 1999, 2011; Kim and O'Neil, 1997). In the case that two secondary minerals are produced in equilibrium from a single fluid phase, the relative degree of O isotopic fractionation can be used to estimate the temperature of the altering fluid (Choi et al., 2000).

We measured the O isotopic compositions of secondary magnetite and carbonates *in situ* in CR chondrites of varying petrologic type to address three main objectives: (1) To quantify the secondary-mineral O-isotope contributions to the whole-rock trend, and determine if these secondary signatures can explain inconsistencies in the whole-rock trend. (2) To understand the O-isotope evolution in minerals and fluids during progressive aqueous alteration. (3) To constrain the temperature of alteration on the CR parent body, and to discern whether the degree of alteration correlates with alteration temperature.

2. ANALYTICAL METHODS

2.1. CR chondrite samples and petrography

A total of nine thin sections from six CR chondrites were used in this work (Table 1). The samples were chosen to represent a wide range of petrologic types, from minimally aqueously altered to nearly completely hydrated. Grosvenor Mountains (GRO) 95577 and Queen Alexandra Range (QUE) 99177 have been described as the hydrated and nominally anhydrous end-members (respectively) of the CR alteration sequence, with both samples containing our desired target minerals within hydrated matrix material (Weisberg and Huber, 2007; Abreu and Brearley, 2010; Schrader et al., 2011, 2014a; Harju et al., 2014; Howard et al., 2015; Abreu, 2016). Elephant Moraine (EET) 92159 (in the EET 87711 pairing group) has also been described as a minimally altered sample in some studies, though not as pristine as QUE 99177 (Schrader et al., 2011; Harju et al., 2014; Abreu, 2016). Renazzo and Al Rais are particularly valuable samples to this study, as they are both moderately altered, containing many primary and secondary phases that essentially record a snapshot of the alteration process (Weisberg et al., 1993; Kallemeyn et al., 1994). Furthermore, Renazzo and Al Rais are both falls and serve as useful diagnostic tools to distinguish products of preterrestrial alteration from minerals formed via weathering. It should be noted that Al Rais is classified as an anomalous CR chondrite, in that it contains an unusually high matrix-plus-dark-inclusion abundance (>70%; Weisberg et al., 1993) compared to other CRs. Lastly, sample MIL 090292 was chosen for this study as it was previously described as being one of only two "fully altered" CRs, along with GRO 95577 (Harju and Rubin, 2013; Harju et al., 2014).

All thin sections were initially studied by optical microscope and mapped using an automated microscopy mapping system developed by Ogliore and Jilly (2013). After carbon-coating, element X-ray maps of each thin section were obtained using the JEOL JXA-8500F electron microprobe at the University of Hawai'i. Calcium, Fe, Mg, Al, and S were measured using a 50 nA beam at 15 kV. Individual elemental maps were combined into multi-element pseudo-mineral maps to identify potential carbonate and magnetite-rich regions for ion microprobe measurements. Sections were then analyzed and imaged using backscattered-electron (BSE) imaging on a JEOL JSM 5900LV scanning electron microscope (SEM) set to an accelerating voltage of 15 kV. Calcite, dolomite, and magnetite grains for O isotope analysis were identified using semi-quantitative energy dispersive X-ray spectroscopy (EDX).

2.2. Secondary Ion Mass Spectrometry (SIMS)

The O isotopic compositions of carbonate and magnetite grains were measured *in situ* using the University of Hawai'i Cameca ims-1280 ion microprobe. Two different analytical setups based upon the methods of Makide et al. (2009) and Nagashima et al. (2015) were used—one for coarse grains (>15 μm) in Renazzo N1127 and GRO 95577, and one for grains smaller than 15 μm, used for

Table 1
List of meteorite thin sections used in this study.

Meteorite	Reported Petrologic Types			Find/Fall	Weathering Grade**
GRO 95577,69	1.3[a]	2.0[b]	1.3[c]	Find	B
MIL 090292,4	–	(2.0)[b]	–	Find	B
MIL 090292,12	–	(2.0)[b]	–	Find	B
Al Rais USNM 6997	2[a]	2.3–an[b]	1.6[c]	Fall (1957)[d]	N/A
Renazzo NHMW-N1126	2.5[a]	2.4[b]	–	Fall (1824)[d]	N/A
Renazzo NHMW-N1127	2.5[a]	2.4[b]	–	Fall (1824)[d]	N/A
EET 92159,20*	2.5[a]	2.8[b]	–	Find	B/C
QUE 99177,69	2.4[a]	2.8[b]	2.8[c]	Find	Be
QUE 99177,06	2.4[a]	2.8[b]	2.8[c]	Find	Be

[a] Petrologic types from Alexander et al., 2013.
[b] Petrologic types from Harju et al., 2014. We argue in this paper that MIL 090292 should not be classified as a CR chondrite. an = anomalous.
[c] Petrologic types from Howard et al., 2015.
[d] Number in parentheses indicates year of fall.
* Paired with EET 87711 and EET 92042.
** Weathering grades for Antarctic meteorites used by the Meteorite Working Group include categories "A," "B," and "C" to denote minor, moderate, and severe rustiness, respectively; "e" indicates the presence of evaporites. There is no weathering scheme for meteorite falls.

the remaining thin sections. For both procedures, a Cs^+ primary beam with total impact energy of 23 keV was used to sputter O isotopes from the sample.

Large grains were presputtered for 90 s to remove the carbon coating and surface contamination using a ~600 pA primary beam focused to ~10 μm and a $10 \times 10\ \mu m^2$ raster. The raster size was then reduced to $7 \times 7\ \mu m^2$ for data collection. Masses $^{16}O^-$, $^{17}O^-$ and $^{18}O^-$ were measured in multicollection mode using a Faraday cup (FC), the axial electron multiplier (EM) and a FC, respectively. The mass resolving power was set to ~2000 for $^{16}O^-$ and $^{18}O^-$ and to ~5000 for $^{17}O^-$, sufficient to resolve the interference from $^{16}OH^-$. Data were collected over 30 cycles to permit monitoring of the ion signals with time and to evaluate their stability. Each cycle ran for 16 s, for a total run time of ~10 min. For grains smaller than ~15 μm, a ~25 pA primary beam was used to obtain a spot size of ~3 μm. All grains were pre-sputtered for 180 s. Because of the low primary beam current, $^{18}O^-$ was measured with an EM, instead of the FC. Each run consisted of 30 cycles of 46 s each, with a total run time of ~25 min. No raster was used for the reduced-beam-size procedure. In both procedures, the $^{16}OH^-$ peak was measured at the end of each measurement. Values of $^{17}O^-$ were corrected for the tail of $^{16}OH^-$ using a tail/peak ratio of 20 ppm, with a typical contribution of ~0.6‰. To assure accuracy of the final results, data gathered by each method was reduced against standard data gathered in the same way.

All ion-probe pits were imaged using the SEM after measurement to ensure that no cracks or different phases were included in the analysis. Any analyses that were clearly mixed or missed the target mineral were discarded. The data were reduced using the method of total counts to minimize statistical bias (Ogliore et al., 2011). All measurement data were converted into delta notation with units of parts per mil (‰), relative to the composition of Vienna standard mean ocean water (VSMOW; Baertschi, 1976; Fahey et al., 1987):

$$\delta^{17,18}O = \left[\left(^{17,18}O/^{16}O\right)_{sample} / \left(^{17,18}O/^{16}O\right)_{VSMOW} - 1\right] \times 1000 \quad (1)$$

The data were also expressed as $\Delta^{17}O$, representing the vertical displacement from the mass-dependent TFL, given in ‰:

$$\Delta^{17}O = \delta^{17}O - 0.52 \times \delta^{18}O \quad (2)$$

Instrumental mass fractionation (IMF) was corrected for via sample-standard bracketing using terrestrial calcite (UWC-1, $\delta^{18}O = 23.36‰$ and UWC-3, $\delta^{18}O = 12.49‰$), terrestrial dolomite (UW6250, $\delta^{18}O = -21.61‰$), and terrestrial magnetite ($\delta^{18}O = -6.05‰$) standards. Standard reproducibility for $\delta^{18}O$ was 0.5‰, 0.4‰, 0.7‰, and 1.1 to 2.0‰ for UWC-1, UWC-3, UW6250, and magnetite standards, respectively; reproducibility for $\delta^{17}O$ was 0.6 to 0.9‰, 1.2‰, 0.8‰, and 1.2 to 1.8‰ (2σ standard deviation). Reported uncertainties on the meteoritic mineral data reflect the propagation of both the internal analytical precision and the external reproducibility of the standards.

3. RESULTS

3.1. Sample petrography

Both calcium carbonate and magnetite are present in all meteorites in this study except the two MIL 090292 sections. No carbonates are present in the MIL 090292 sections, though magnetite is abundant. The Ca carbonate found in the CR samples is stoichiometrically $CaCO_3$ as determined by EDX and electron microprobe analysis (Jilly-Rehak et al., 2017). We will assume that the $CaCO_3$ phase here is calcite, rather than aragonite, since calcite has been reported in other studies of CR chondrites (e.g., Brearley, 2006 and references therein). Dolomite was found in dark inclusions from two thin sections, Renazzo N1126 and EET 92159,20. Petrographic descriptions of each meteorite in this study are included in the Supplemental Material, which provide a basis for later discussions.

3.2. Oxygen isotopes

The O-isotope dataset in this study consists of 51 calcite analyses, five dolomite analyses, and 50 magnetite analyses. A linear least-squares regression through all calcite yields a slope of 0.64 ± 0.04, $\chi^2_{red} = 1.1$ (Fig. 1a), where the $\Delta^{17}O$ values range from ~3 to −3‰ (Fig. 1b). Similarly, a regression through the magnetite data from CR chondrites (not including MIL 090292, see discussion) yields a slope of 0.63 ± 0.05, $\chi^2_{red} = 0.9$ (Fig. 1a), with $\Delta^{17}O$ values ranging from ~2 to −3‰ (Fig. 1b). The dolomite $\Delta^{17}O$ values range from ~0 to −2‰, with no apparent correlation between $\Delta^{17}O$ and $\delta^{18}O$. We detail the results from each meteorite below.

3.2.1. Oxygen isotopes in calcite

We analyzed calcite grains in six CR chondrite thin sections from four different meteorites (Table 2); characteristic ion probe pits for each meteorite are shown in Fig. 2. While calcite is present in EET 92159, the grains were too small for SIMS analysis. No calcite is present in MIL 090292. The calcite measurements plot near the TFL and show a large spread in $\delta^{18}O$ with a range from 9‰ to 35‰ (Fig. 3). Calcite O isotopes form a distinct array for each meteorite. The GRO 95577 analyses are tightly clustered around $\delta^{18}O \approx 19‰$, and $\Delta^{17}O \approx 0‰$ (Fig. 3 inset). In contrast, calcite in Al Rais, Renazzo, and QUE 99177 plot on arrays of variable $\delta^{18}O$. The Al Rais calcites have the heaviest O isotopic compositions of all minerals measured here, with $\delta^{18}O$ ranging from 29‰ to 35‰. The average $\Delta^{17}O = 0.8‰$ for Al Rais, and there is no resolved correlation between $\delta^{18}O$ and $\Delta^{17}O$. For Renazzo N1126 and N1127, $\delta^{18}O$ ranges from approximately 16 to 30‰. The $\delta^{17}O$ values correlate with $\delta^{18}O$, forming an array with a linear least-squares regression slope of 0.71 ± 0.10 (2σ) on an O three-isotope diagram (Fig. 3). This trend translates into a trend with a slight positive slope on a $\Delta^{17}O$ vs $\delta^{18}O$ plot (Fig. 1b). The QUE 99177 calcite grains plot on a linear array ranging from $\delta^{18}O = 9$ to 25‰. Two calcite grains from a hydrated region of the matrix define the end of this array near $\delta^{18}O = 9‰$, while the majority of the grains have

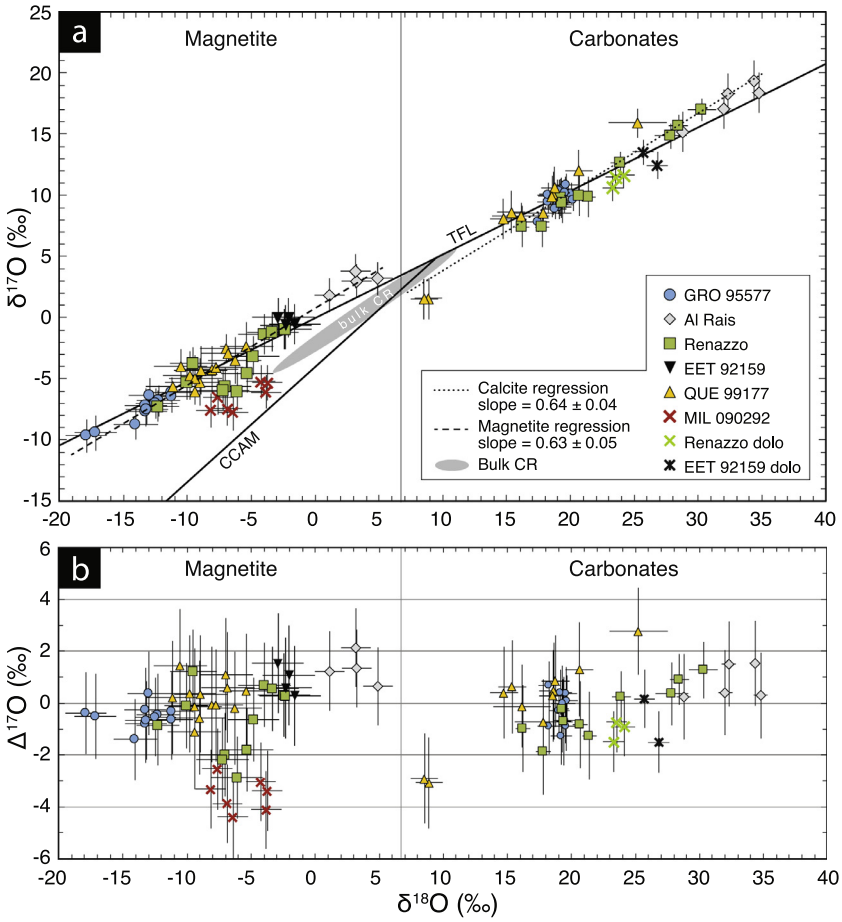

Fig. 1. Comparison of carbonate and magnetite O isotopes from CR chondrites. (a) Oxygen three-isotope plot depicting $\delta^{17}O$ vs. $\delta^{18}O$. The shaded region represents the whole-rock O isotope trend for CR chondrites (Clayton and Mayeda, 1999; Schrader et al., 2011). The regression for the magnetite data does not include MIL 090292, and the calcite regression does not include dolomite data. (b) Plot of $\Delta^{17}O$ vs. $\delta^{18}O$ for all meteorites. For magnetite, there is an overall positive slope where $\Delta^{17}O$ correlates with $\delta^{18}O$ (excluding MIL 090292, see discussion); however, individual meteorites do not show a correlation. The calcite dataset as a whole also shows an overall increase of $\Delta^{17}O$ with $\delta^{18}O$. For individual meteorites, both Renazzo and QUE 99177 exhibit $\Delta^{17}O$ correlations with $\delta^{18}O$. All uncertainties are 2σ.

$\delta^{18}O \geq 14‰$. The O isotopes form an array of slope 0.86 ± 0.13 (2σ) on an O three-isotope diagram. Here again, $\Delta^{17}O$ correlates with $\delta^{18}O$ (Fig. 1b). The arrays for Renazzo and QUE 99177 are statistically distinct from a slope-0.5 mass-dependent fractionation trend.

3.2.2. O isotopes in dolomite

Dolomite grains are relatively uncommon in CR chondrites, and were only found in two thin sections, Renazzo N1126 and EET 92159,20. Five O-isotope analyses were made on dolomite grains in the two thin sections (Table 3; Fig. 2e and f). The O compositions cluster near the TFL, with the data averaging $\delta^{18}O = 23.7‰$ for Renazzo, and $\delta^{18}O = 26.3‰$ for EET 92159 (Fig. 4). The average of the data for both meteorites plots below the TFL.

3.2.3. O isotopes in magnetite

We analyzed magnetite grains in eight thin sections representing six different CR chondrites for O isotopes (Table 4); characteristic ion probe pits are shown in Fig. 5. Most magnetite O isotopes have negative values relative to SMOW on the O three-isotope diagram, with the total $\delta^{18}O$ ranging from −18 to 5‰ (Fig. 6). Each meteorite exhibits a distinct array, with some overlapping regions. The GRO 95577 magnetite array ranges from $\delta^{18}O = -11$ to −17‰, with a $\Delta^{17}O$ value of ~−0.5‰. Matrix spherules from Al Rais are the isotopically heaviest magnetite grains, and the only grains with positive $\delta^{18}O$ values (from 1‰ to 5‰). The average $\Delta^{17}O$ is 1.3‰, slightly above the TFL. The magnetite from Renazzo N1127 is represented by one grain from a dark inclusion ($\delta^{18}O = -10.1‰$) and one altered metal nodule from a chondrule ($\delta^{18}O = -12.3‰$). Both grains have $\Delta^{17}O \sim 0‰$. Magnetite analyses from a chondrule rim in Renazzo N1126 form an array from $\delta^{18}O = -2.5$ to −4‰, and $\Delta^{17}O \approx 0‰$. Five magnetite analyses from a dark inclusion in Renazzo N1126 fall slightly below the CR trend at $\Delta^{17}O \approx -1.9‰$. In EET 92159,20, magnetite from the dark inclusion lithology was measured, as no large magnetite grains were found in the host matrix. Values cluster near $\delta^{18}O \sim -6‰$ and $\Delta^{17}O$

Table 2
Secondary calcite oxygen isotope results from CR chondrites. All values reported in permil deviation from SMOW (‰). Measurements are shown in order of increasing $\delta^{18}O$.

Thin Section	$\delta^{18}O$[a]	2σ	$\delta^{17}O$[a]	2σ	$\Delta^{17}O$[a]	2σ	Grain	Lithology
GRO 95577,69 (CR 2.0)	17.4	±0.9	7.8	±0.8	−1.3	±1.0	C22	Chondrule mesostasis
	18.3	±0.9	10.0	±1.1	0.5	±1.2	C10	Matrix
	18.3	±0.9	9.5	±0.9	0.0	±1.0	C05	Matrix
	18.8	±0.9	8.9	±0.8	−0.9	±0.9	C21	Chondrule mesostasis
	19.0	±0.9	10.4	±0.9	0.5	±1.0	C11	Matrix
	19.1	±0.8	9.3	±0.8	−0.6	±0.9	C01	Matrix
	19.1	±0.7	10.3	±0.9	0.4	±1.0	C20	Chondrule mesostasis
	19.1	±0.9	9.7	±1.0	−0.3	±1.1	C12	Matrix
	19.1	±1.0	9.0	±0.9	−0.9	±1.1	C13a	Matrix
	19.1	±0.9	9.8	±1.1	−0.1	±1.2	C13b	Matrix
	19.1	±0.9	10.0	±0.9	0.1	±1.0	C06	Matrix
	19.2	±0.9	10.2	±1.1	0.2	±1.2	C08	Matrix
	19.2	±1.0	9.2	±0.9	−0.8	±1.1	C14	Matrix
	19.3	±0.9	10.1	±0.8	0.1	±0.9	C16	Chondrule mesostasis
	19.3	±0.8	10.4	±1.0	0.4	±1.1	C18	Chondrule mesostasis
	19.4	±0.9	10.1	±0.9	0.0	±1.0	C09	Matrix
	19.5	±0.9	9.5	±0.9	−0.7	±1.0	C17	Chondrule mesostasis
	19.6	±0.9	10.2	±0.9	0.0	±1.0	C03	Matrix
	19.6	±0.9	10.5	±1.0	0.4	±1.1	C04	Matrix
	19.6	±1.0	10.2	±0.9	0.0	±1.0	C07	Matrix
	19.6	±0.9	10.2	±0.8	0.0	±0.9	C23	Matrix
	19.6	±0.9	10.3	±1.0	0.0	±1.1	C02	Matrix
	19.6	±1.0	10.9	±0.8	0.7	±1.0	C19	Chondrule mesostasis
	20.1	±0.9	10.1	±0.8	−0.3	±0.9	C15	Chondrule mesostasis
	20.2	±0.8	9.6	±0.9	−0.9	±1.0	C24	Matrix
Al Rais USNM 6997 (CR 2.3)	28.8	±0.5	15.2	±1.6	0.2	±1.6	C02	Matrix
	32.0	±0.5	17.0	±1.6	0.4	±1.6	C03b	Matrix
	32.3	±0.5	18.3	±1.6	1.5	±1.6	C03a	Matrix
	34.3	±0.4	19.4	±1.6	1.5	±1.6	C04	Matrix
	34.8	±0.6	18.4	±1.6	0.3	±1.7	C01	Matrix
Renazzo N1126 (CR 2.4)	16.2	±0.6	7.5	±1.6	−1.0	±1.7	C03b	Matrix
	17.8	±0.6	7.4	±1.7	−1.9	±1.7	C01a	Matrix
	19.3	±0.6	9.8	±1.6	−0.2	±1.7	C01b	Matrix
	19.4	±0.6	9.4	±1.7	−0.7	±1.7	C03a	Matrix
	20.7	±0.6	9.9	±1.7	−0.8	±1.7	C04b	DI
	21.4	±0.6	9.9	±1.7	−1.3	±1.7	C04a	DI
Renazzo N1127 (CR 2.4)	23.9	±0.7	12.7	±0.9	0.2	±1.0	C02	Matrix
	27.9	±1.3	14.9	±1.0	0.4	±1.2	C04a	Matrix
	28.4	±0.7	15.7	±0.9	0.9	±1.0	C04b	Matrix
	30.3	±1.1	17.0	±0.9	1.3	±1.1	C01	Matrix
QUE 99177,06 (CR 2.8)	8.5	±1.1	1.5	±1.7	−2.9	±1.7	C07	Matrix
	8.9	±1.1	1.6	±1.7	−3.1	±1.8	C06	Matrix
	14.7	±1.1	8.1	±1.7	0.4	±1.8	C02b	Matrix
	15.4	±1.1	8.6	±1.7	0.6	±1.8	C02c	Matrix
	18.6	±1.1	9.9	±1.7	0.3	±1.8	C01b	Matrix
	18.6	±1.1	10.2	±1.8	0.5	±1.9	C02a	Matrix
	18.8	±1.1	10.6	±1.7	0.9	±1.8	C01a	Matrix
	20.6	±1.1	12.0	±1.7	1.3	±1.8	C08	DI
QUE 99177,69 (CR 2.8)	16.1	±2.2	8.3	±1.1	−0.1	±1.6	C01c	DI
	17.8	±2.2	8.6	±1.1	−0.7	±1.6	C01b	DI
	25.2	±2.3	15.9	±1.2	2.8	±1.7	C04	Chondrule rim/Matrix

[a] All reported uncertainties are 2σ.

~1‰. In both sections of QUE 99177, the magnetite plots on a trend along the TFL, ranging from $\delta^{18}O = -5$ to −11‰. Magnetite in MIL 090292,12 has a composition that falls off of the trend defined from the other CR chondrites. The average $\Delta^{17}O$ value is significantly lower at ~−3‰, falling below even the magnetite in the Renazzo N1126 dark inclusion. The $\delta^{18}O$ values range from −8.2 to −3.7‰. None of the individual meteorites show a correla-

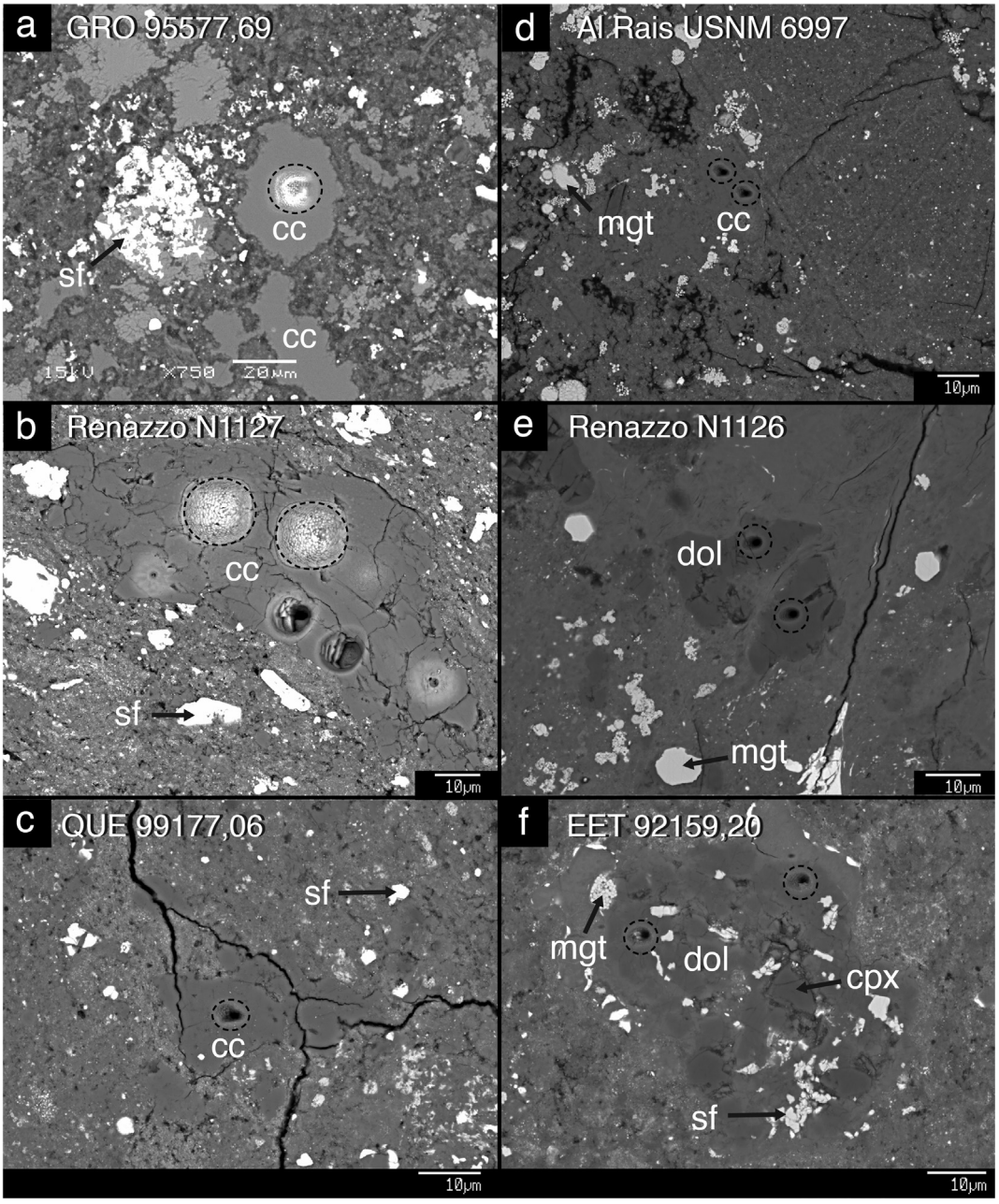

Fig. 2. BSE images of characteristic ion probe pits in carbonates, shown in dashed circles. (a) Analysis C09 from GRO 95577,69. (b) Analyses C04a,b from Renazzo N1127. Other holes are from Mn and Cr measurements in a separate study. (c) Analysis C08 from QUE 99177,06. (d) Analyses C03a,b from Al Rais USNM 6997. (e) Analyses D01a,b from Renazzo N1126. (f) Analyses D01a,b from EET 92159,20. cc = calcite, cpx = clinopyroxene, dol = dolomite, mgt = magnetite; sf = sulfide.

tion between $\Delta^{17}O$ and $\delta^{18}O$, though there is a slight positive slope for the complete dataset (Fig. 1b).

4. DISCUSSION

In this section, we discuss the significance of the O isotopic trends measured from calcite, dolomite, and magnetite in CR chondrites of varying petrologic type. First, we discuss the potential influence of terrestrial weathering on O isotopes, and conclude that the minerals measured here were not significantly weathered and retain their extra-terrestrial signatures. The O isotopic composition of all minerals plot on trends near the TFL, with the exception of magnetite in MIL 090292, which we interpret as an anomalous specimen (cf. Section 4.2 below). We find that the average O isotopic compositions of secondary minerals do not correlate with the petrologic types of the host specimens, but may instead depend on the lithology being measured. This lithologic diversity of CR chondrites can account for inconsistencies in the bulk O trend, as the bulk

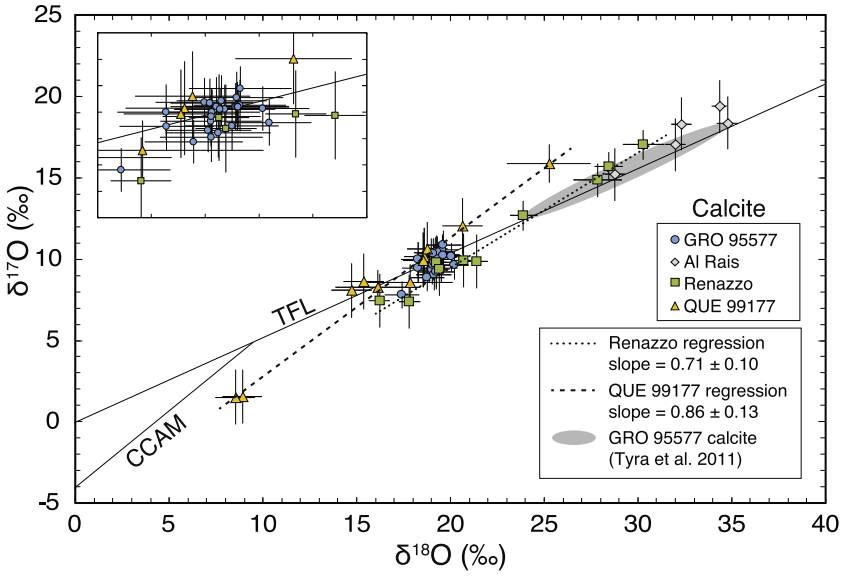

Fig. 3. Calcite O isotopes from GRO 95577, Al Rais, Renazzo, and QUE 99177. Plotted for reference are the terrestrial fractionation line (TFL) and the carbonaceous chondrite anhydrous mineral line (CCAM). The majority of GRO 95577 calcites plot in a tightly clustered area of the graph, shown in the inset graph where $\delta^{18}O$ ranges from 17‰ to 22‰. Uncertainties are 2σ. Weighted linear regressions for QUE 99177 and Renazzo mass independent trends show the correlation between $\Delta^{17}O$ and $\delta^{18}O$.

Table 3
Secondary dolomite oxygen isotope results from CR chondrites. All values reported in permil deviation from SMOW (‰). Measurements are shown in order of increasing $\delta^{18}O$.

Thin Section	$\delta^{18}O$[a]	2σ	$\delta^{17}O$[a]	2σ	$\Delta^{17}O$[a]	2σ	Grain	Lithology
Renazzo N1126	24.2	±0.8	11.7	±1.1	−0.9	±1.1	D01a	DI
	23.5	±0.8	11.5	±1.1	−0.7	±1.1	D01b	DI
	23.3	±0.8	10.6	±1.1	−1.5	±1.2	D02b	DI
EET 92159,20	26.8	±0.8	12.4	±1.1	−1.5	±1.2	D01a	DI
	25.7	±0.8	13.5	±1.0	0.2	±1.1	D01b	DI

[a] All reported uncertainties are 2σ.

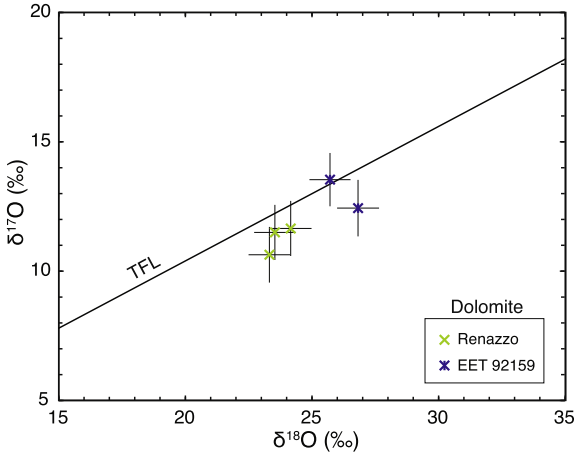

Fig. 4. Dolomite O isotopes from Renazzo N1126 and EET 92159,20. The TFL is plotted for reference. Uncertainties are 2σ.

O isotopes represent an amalgamation of different generations of alteration, scattered by impacts as lithic clasts, and in some cases overprinted by additional *in situ* alteration. Using equilibrium O-isotope partitioning in calcite and magnetite, we find that alteration temperatures were low (~60 °C) and that the fluid composition evolved significantly on the CR parent body.

4.1. Influence of terrestrial weathering

Terrestrial weathering is of great concern for studies of aqueous alteration, as many of the secondary products produced by weathering on earth are similar to minerals that formed during parent-body alteration (Bland et al., 2000, 2006; Tyra et al., 2007). A terrestrial origin of the secondary minerals measured here must be ruled out, since many of the O isotopic compositions lie near the TFL. Renazzo and Al Rais, both witnessed falls, are important to this study as they have largely escaped terrestrial weathering, and provide a baseline for distinguishing parent body and terrestrial alteration products.

The remaining meteorites in this study are Antarctic finds of weathering grade B, with likely residence times of tens to hundreds of thousands of years (Nishiizumi et al., 1989; Bland et al., 2006). For the majority of their Antarctic

Table 4
Secondary magnetite oxygen isotope results from CR chondrites. All values reported in permil deviation from SMOW (‰). Measurements are shown in order of increasing $\delta^{18}O$.

Thin Section	$\delta^{18}O$[a]	2σ	$\delta^{17}O$[a]	2σ	$\Delta^{17}O$[a]	2σ	Grain	Lithology
GRO 95577,69 (CR 2.0)	−17.9	±1.6	−9.7	±1.3	−0.4	±1.6	M01b	Chondrule nodule
	−17.2	±1.6	−9.4	±1.4	−0.5	±1.6	M15	Chondrule nodule
	−14.0	±1.7	−8.7	±1.3	−1.4	±1.6	M01a	Chondrule nodule
	−13.3	±1.6	−7.1	±1.4	−0.3	±1.6	M04	Chondrule nodule
	−13.2	±1.6	−7.7	±1.3	−0.8	±1.5	M06a	Chondrule nodule
	−13.2	±1.6	−7.5	±1.2	−0.7	±1.5	M06b	Chondrule nodule
	−13.0	±1.7	−6.4	±1.4	0.4	±1.6	M02	Chondrule nodule
	−12.5	±1.6	−7.0	±1.3	−0.5	±1.5	M14	Chondrule nodule
	−12.3	±1.7	−6.8	±1.3	−0.4	±1.6	M11z	Chondrule nodule
	−11.2	±1.7	−6.5	±1.3	−0.6	±1.5	M11b	Chondrule nodule
	−11.2	±1.6	−6.1	±1.2	−0.3	±1.5	M08	Chondrule nodule
MIL 090292,12 (CR 2.0)	−8.2	±1.2	−7.6	±1.4	−3.3	±1.5	M03	Chondrule nodule
	−7.6	±1.2	−6.5	±1.4	−2.5	±1.6	M02b	Chondrule nodule
	−6.9	±1.2	−7.4	±1.4	−3.9	±1.5	M04	Chondrule nodule
	−6.4	±1.2	−7.7	±1.5	−4.4	±1.6	M01b	Chondrule nodule
	−4.2	±1.2	−5.2	±1.4	−3.0	±1.5	M02a	Chondrule nodule
	−3.8	±1.2	−6.1	±1.4	−4.1	±1.5	M01a	Chondrule nodule
	−3.7	±1.2	−5.3	±1.4	−3.4	±1.5	M05	Chondrule nodule
Al Rais USNM 6997 (CR 2.3)	1.1	±1.2	1.8	±1.4	1.2	±1.5	M04	Matrix
	3.2	±1.2	3.8	±1.4	2.1	±1.5	M03	Matrix
	3.2	±1.2	3.0	±1.4	1.3	±1.5	M01	Matrix
	4.9	±1.2	3.2	±1.4	0.7	±1.5	M02	Matrix
Renazzo N1126 (CR 2.4)	−7.2	±2.0	−6.0	±1.6	−2.2	±1.9	M03	DI
	−7.0	±2.0	−5.7	±1.6	−2.0	±1.9	M02	DI
	−6.1	±2.0	−6.0	±1.6	−2.9	±1.9	M01	DI
	−5.3	±2.0	−4.5	±1.6	−1.8	±1.9	M04b	DI
	−4.8	±2.0	−3.1	±1.6	−0.6	±1.9	M04a	DI
	−4.0	±2.0	−1.4	±1.6	0.7	±1.9	M06	Chondrule rim (in clast)
	−3.3	±2.0	−1.2	±1.6	0.5	±1.9	M08	Chondrule rim (in clast)
	−2.4	±2.0	−1.0	±1.6	0.3	±1.9	M05	Chondrule rim (in clast)
	−2.3	±2.0	−1.0	±1.6	0.3	±1.9	M07	Chondrule rim (in clast)
Renazzo N1127 (CR 2.4)	−12.3	±1.7	−7.2	±1.3	−0.9	±1.5	M01	Chondrule nodule
	−10.1	±1.7	−5.3	±1.4	−0.1	±1.6	M05	DI
EET 92159,20 (CR 2.8)	−2.9	±2.0	0.0	±1.6	1.5	±1.9	M03	Chondrule rim
	−2.3	±2.0	−0.6	±1.6	0.6	±1.9	M01	Chondrule rim
	−2.1	±2.0	0.0	±1.6	1.1	±1.9	M04	Chondrule rim
	−1.6	±2.0	−0.5	±1.6	0.3	±1.9	M02	Chondrule rim
QUE 99177,06 (CR 2.8)	−9.8	±2.1	−4.7	±2.0	0.4	±2.3	M04a	DI
	−9.4	±2.1	−5.0	±1.9	−0.1	±2.2	M03	DI
	−9.0	±2.1	−5.3	±1.9	−0.6	±2.2	M02b	DI
	−8.9	±2.1	−4.3	±2.0	0.4	±2.3	M04d	DI
	−8.1	±2.1	−4.3	±1.9	−0.1	±2.2	M01	DI
	−6.3	±2.1	−3.5	±1.9	−0.2	±2.2	M04b	DI
	−5.4	±2.1	−2.3	±1.9	0.5	±2.2	M02a	DI
QUE 99177,69 (CR 2.8)	−11.2	±2.1	−5.6	±1.9	0.2	±2.2	M03a	DI
	−10.5	±2.1	−4.0	±1.9	1.5	±2.2	M03b	DI
	−9.4	±2.1	−6.0	±1.9	−1.1	±2.2	M01	DI
	−7.7	±2.1	−4.1	±1.9	−0.1	±2.2	M02a	DI
	−7.0	±2.1	−2.5	±1.9	1.1	±2.2	M02b	DI
	−6.8	±2.1	−3.0	±1.8	0.6	±2.1	M02c	DI

[a] All reported uncertainties are 2σ.

residence, the meteorites were likely trapped in glacial ice sheets, preserving the stone in its original state (Cassidy et al., 1992). However, once the meteorites were exhumed from the ice by the Antarctic winds, freeze–thaw cycling would have subjected the meteorites to liquid water that causes terrestrial weathering. Antarctic glacial ice and melt-water has extremely negative values of $\delta^{18}O \sim -50$ to −35‰ (Gooding, 1986; Aharon, 1988; Faure et al.,

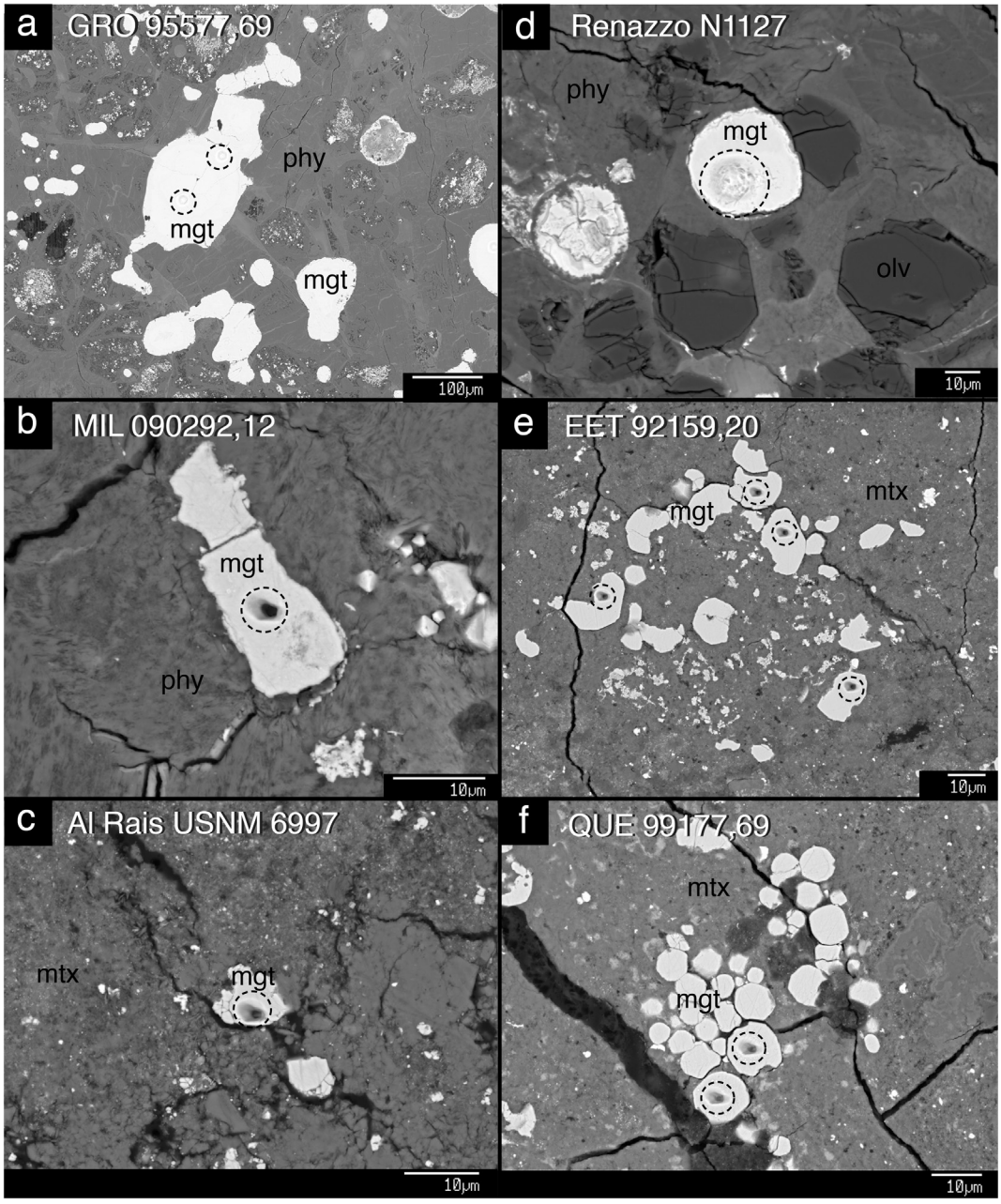

Fig. 5. BSE images of characteristic ion probe pits in magnetite (dashed circles). (a) Analyses M06a,b from GRO 95577,69. (b) Analysis M05 in MIL 090292,12. (c) Analysis M04 from Al Rais USMN 6997. (d) Analysis M01 from Renazzo N1127. (e) Analyses M01, M02, M03, M04 from EET 92159,20. (f) Analyses M03a,b from QUE 99177,69. mgt = magnetite; mtx = matrix; olv = olivine; phy = phyllosilicate.

1988), suggesting that even small contamination could lead to changes in the measured O isotopes. Yet surprisingly, a significant amount of Antarctic weathering (>25% oxidation of iron) is required before any significant isotopic effect is observed in the bulk O isotopic compositions (Bland et al., 2000, 2006). A similar finding has been established for H, C, and N in CM and CR meteorites, where falls and weathered finds show similar ranges in isotopic composition with no correlation between weathering grade and bulk composition (Alexander et al., 2012, 2013).

Iron oxidation products (e.g., rust or ferrihydrite) are the most obvious signs of terrestrial weathering for CR chondrites. Most Antarctic CR chondrites contain networks of iron-oxyhydroxide veins that fill in cracks, fractures, and follow grain boundaries in chondrules (Abreu and Brearley, 2010). TEM studies of vein cross-sections have shown that the weathering remains restricted to the alteration veins with minimal effects on the surrounding material (Abreu and Brearley, 2010). Some metal grains in Renazzo and Al Rais exhibit minor rust halos, but the

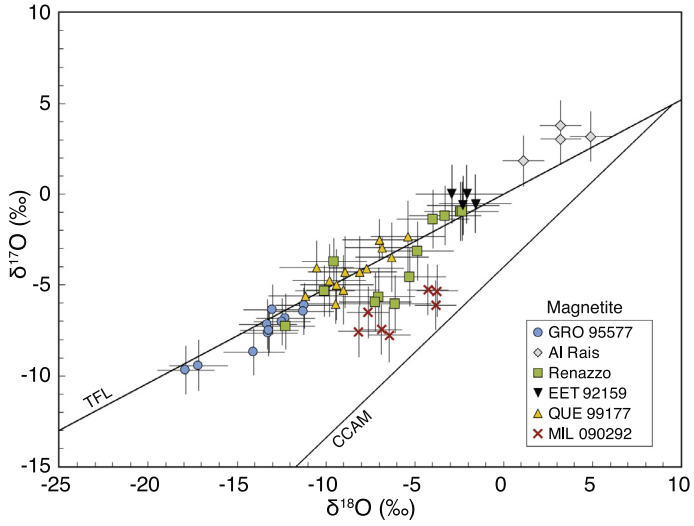

Fig. 6. Magnetite O isotopes from eight thin sections in this study. Each meteorite forms a separate array with a spread of 3–6‰. While most magnetite grains plot on an array near the TFL, magnetite grains from MIL 090292,12 have low $\Delta^{17}O$ values. Uncertainties are 2σ.

sections are otherwise free of iron oxide veins. Most metal grains in CR chondrites display pre-terrestrial oxide rims composed of magnetite, rather than the common weathering products ferrihydrite or goethite (Bland et al., 2006). Magnetite is an extremely uncommon product of Antarctic terrestrial weathering (Bland et al., 1998, 2006) supporting a pre-terrestrial origin for the magnetite measured here.

Carbonates have been noted as a common product of terrestrial weathering, usually occurring as hydrous magnesium carbonates (Velbel et al., 1991; Bland et al., 2006) and possibly calcium carbonates (Abreu and Brearley, 2005). Carbonates formed from Antarctic waters have $\delta^{18}O$ values ranging from −47 to 4.5‰ (Hays and Grossman, 1991; Rao et al., 1998). Low $\delta^{18}O$ values in terrestrial carbonates reflect the formation from highly negative $\delta^{18}O$ glacial melt-water at low temperatures (Hanshaw and Hallet, 1978; Faure et al., 1988; Hays and Grossman, 1991; Zheng, 2011). Compared to carbonates in Al Rais and Renazzo, two relatively unweathered falls, the calcite and dolomite measured in GRO 95577, EET 92159, and QUE 99177 do not exhibit the extreme negative $\delta^{18}O$ values that would be expected for Antarctic precipitates (e.g., Gooding, 1986; Hays and Grossman, 1991; Tyra et al., 2011; Zheng, 2011). While Al Rais does have the highest $\delta^{18}O$ values measured in this study, the Renazzo carbonates have $\delta^{18}O$ values that cover nearly the same range as the carbonates in the Antarctic finds. A lack of carbonates with highly negative $\delta^{18}O$ values may not necessarily stand as proof against weathering, however. Some Antarctic CM chondrites contain carbonates that have exchanged O isotopes, thus forming a unique array that intersects the trend for carbonates in CM falls and the terrestrial fractionation line (Tyra et al., 2007). No similar trend was observed for the Antarctic CR carbonates measured in this study. The magnetite and carbonate O isotopes plot on the same general trend as Al Rais, and in arrays that overlap the Renazzo secondary mineral compositions.

Instances of terrestrial calcite have been reported in some meteorite falls, suggesting that carbonate formation can occur even within months of exposure (Abreu and Brearley, 2005). Such terrestrial calcites may manifest as long veins extending up to hundreds of microns. However, some key characteristics of the Renazzo veins set them apart from terrestrially-formed veins. First, the O isotopic compositions of some Renazzo calcite veins do not lie on the terrestrial fractionation line, indicating formation from an O reservoir that was clearly not terrestrial. Renazzo veins do not cross-cut the meteorite components; they are only found in hydrated matrix. The calcite veins in Renazzo are compositionally homogeneous (cf. Supplementary Material Fig. S3), and do not show elemental zoning or co-precipitation with terrestrial iron oxides, as seen in terrestrial carbonate veins (Abreu and Brearley, 2005). Finally, the Renazzo calcite veins do not fill in cracks in the meteorite, nor are carbonates found in the pore space of the fusion crust or on the exterior of the meteorite.

While these petrographic observations provide ample evidence for pre-terrestrial alteration, perhaps the most convincing evidence lies in radiometric dating. ^{53}Mn-^{53}Cr dating of carbonate grains in Renazzo and GRO 95577 indicates that ^{53}Mn ($t_{1/2} = 3.7$ Myr) was still present at the time of calcite formation. The resolvable Mn-Cr isochrons are evidence that the carbonates formed between ~2 to 13 Myr after the formation of Ca-Al-rich inclusions (CAIs), at >4.55 Ga (Jilly-Rehak et al., 2017). Many of the the Renazzo and GRO 95577 carbonates measured here for O isotopes were subsequently measured for the Mn-Cr study, avoiding contamination of the O isotopes by the $^{16}O^-$ beam used in the radiometric dating technique.

4.2. Distinct properties of MIL 090292

Many properties of MIL 090292 suggest that this sample is anomalous or unrelated to the CR chondrite group. MIL

090292 has been classified as a CR 2.0 (Harju et al., 2014) based upon its high abundance of secondary minerals, including phyllosilicates, magnetite, and sulfides (Satterwhite and Righter, 2012; Harju et al., 2014). Magnetite-bearing chondrule pseudomorphs indicate that the precursor chondrules were metal-rich, similar to the chondrules in CR chondrites. However, an important mineralogical difference is that the chondrule magnetite in MIL 090292 contains abundant small 1 to 6 μm grains of Ni-rich metal (~88 wt% Ni, 12 wt% Fe). This Ni-rich metallic phase is not seen in other CR chondrites, suggesting that the alteration conditions or O fugacity for MIL 090292 were unique. Cubanite is another phase in MIL 090292 that is not present in other CR chondrites (Brearley, 2006; Schrader et al., 2015). Similarly, MIL 090292 does not contain Ca-carbonates, a common phase in all other CR chondrite specimens, particularly in heavily altered lithologies (e.g., Schrader et al., 2014a). Rather, Ca resides in secondary Ca-phosphates and in Ca-Fe-rich silicates (andradite and hedenbergite, also never reported in CR chondrites, but which occur in CV chondrites; Krot et al., 1998). The lack of carbonate phases may be indicative of different alteration conditions such as lower pH, higher Si activity, or higher temperatures (e.g., Krot et al., 1998, 2000; Jilly and Huss, 2012).

The O-isotopes from MIL 090292 consistently diverge from established CR trends. Magnetite O-isotopes reported here (with $\Delta^{17}O \sim -3.5‰$) plot outside of the array defined by all other CR magnetite. This negative $\Delta^{17}O$ value is similar to magnetite in some CV, CO and CK chondrites (Choi et al., 1997; Choi and Wasson, 2003; Hsu et al., 2006; Jogo et al., 2011; Davidson et al., 2014; Doyle et al., 2015; Krot and Nagashima, 2016). The whole-rock O isotopic composition of MIL 090292 measured by Harju et al. (2014) fell off of the slope-0.7 CR mixing line, near the CCAM line. Similar whole-rock and matrix-separate analyses from Schrader et al. (2014a) show that MIL 090292 plots distinctly lower on the bulk CR trend than would be expected for an extensively altered CR. These observations suggest that MIL 090292 is not a CR chondrite, or at the very least, has an anomalous origin, and alteration occurred under unique fluid conditions.

4.3. Carbonate O isotopes: A proxy for fluid evolution on the CR parent body

The variability in O isotopic composition between carbonate grains measured here indicates that the carbonates in all CR chondrites did not form from a single uniform fluid on the parent body. Previous studies of carbonates in carbonaceous chondrites show that each grain likely formed in local equilibrium with its own associated fluid (e.g., Riciputi et al., 1994; Benedix et al., 2003). Therefore, the compositions of the carbonate grains essentially serve as a proxy for fluid chemistry at the time of carbonate precipitation, and variations in grain composition likely reflect evolving conditions or compositions of the altering fluid itself.

In any water–rock reaction, there are four main influences on the isotopic composition: the temperature, the water/rock (W/R) ratio, the original composition of the fluid, and the original composition of the rock (Taylor, 1977; Agrinier and Cannat, 1997). For terrestrial minerals, all of these influences result in O isotopic fractionation along the TFL, which has a slope of 0.52 on the O three-isotope diagram. Oxygen isotopic fractionation in extraterrestrial materials is more complicated, as the interaction between materials from distinct O isotopic reservoirs can lead to arrays that do not follow a slope-0.52 trend. Mass-dependent fractionation trends (i.e., slope-0.52 trends) in secondary minerals can be attributed to variation in temperature, or to variation in fluid composition as a result of equilibrium fractionation between the water and precipitating minerals such as calcite (e.g., Clayton and Mayeda, 1984; Young et al., 1999). Mass-independent trends (i.e., variable $\Delta^{17}O$) arise from processes that do not depend on mass, such as O isotope exchange between, or mixing of two different O isotopic reservoirs. The slope of a data array on the O three-isotope diagram can therefore reveal information about fluid chemistry and conditions of aqueous alteration (e.g., Clayton and Mayeda, 1984, 1999; Benedix et al., 2003; Schrader et al., 2011).

The calcite O-isotope arrays differ for each meteorite in this study (Fig. 3). All GRO 95577 calcite grains were measured from the hydrated lithology, where 21 analyses were matrix grains and 11 analyses were from pseudomorphed chondrule mesostasis. All calcite grains in GRO 95577 have the same compositions (within error), suggesting that they were formed under uniform physico-chemical conditions. The measured O-isotope composition ($\delta^{18}O \sim 19‰$) is not the same as those of calcite measured in other sections of GRO 95577 (Tyra et al., 2011), which spanned an array near the TFL from $\delta^{18}O \sim 25$ to 35‰ (see Fig. 3). The calcite measurements in Tyra et al. (2011) were taken from three lithologies across two thin sections, showing that the composition varied between the different lithologies. The different results from these two studies likely reflect the heterogeneity of lithologic components in this meteorite. Fluids were locally uniform during carbonate precipitation in the hydrated region where the GRO 95577,69 carbonates formed. To reconcile the Tyra et al. (2011) data, the O isotopes must have been fractionated mass-dependently (since all $\Delta^{17}O \sim 0‰$) on a larger spatial and/or temporal scale. Each lithology may have been altered under different fluid conditions (e.g., different fluid temperatures) on the parent body and then subsequently transported via impact processes. Alternatively, alteration may have varied at the scale of a few inches, potentially due to low permeability, such that different thin sections of the same meteorite capture different fluid conditions.

Al Rais calcite grains measured here were located in the fine-grained matrix of a single lithology (e.g., Fig. 2d). The calcite O compositions show no resolvable variation in $\Delta^{17}O$. This may indicate that isotopic exchange between the water and rock reservoir(s) with different $\Delta^{17}O$ was minimal within the locality sampled in the thin section, or that isotopic exchange was complete. The calcite compositions plot above the terrestrial fractionation line and have the most positive average $\Delta^{17}O$ (Fig. 1). In the context of a model where the altering fluid has a higher $\Delta^{17}O$ than the

rock (e.g., Clayton and Mayeda, 1984, 1999), the relatively high $\Delta^{17}O$ might indicate minimal isotopic exchange with the solids with negative $\Delta^{17}O$ compositions prior to carbonate precipitation. The variation in $\delta^{18}O$ can either be interpreted as changing temperature during progressive alteration, or variable fluid isotopic composition due to equilibrium fractionation during the precipitation of calcite or other phases. In the case of variable composition, the fluid would evolve toward a lighter isotopic composition as carbonates precipitate.

Calcite in Renazzo was measured from two distinct lithologies: eight analyses within the fine-grained interchondrule matrix, and two analyses from a dark inclusion. The data form a single array with a slope of ~0.7 (Fig. 3), indicating that both lithologies were altered by a single evolving fluid on the CR parent body. Previous studies have suggested that the dark inclusions may have originated from an exogenous source outside of the CR parent body (Endreß et al., 1994). However, the similarity in O isotopes indicate that the dark inclusions measured here come from a nearby region on the CR parent body, transported by impacts, rather than being foreign clasts from an exogenous source (e.g., Weisberg et al., 1993). The trend for the Renazzo calcites likely represents a mixture of mass-dependent and mass-independent processes. Variations in $\Delta^{17}O$ suggest that some degree of isotopic exchange occurred between ^{16}O-depeleted water and ^{16}O-enriched solid materials during progressive alteration, while variations in $\delta^{18}O$ likely reflect changes in temperature. The dolomite O isotopes from a dark inclusion in Renazzo N1126 plot within the calcite array, but show no indication of chemical or temperature evolution during formation. However, the dolomite data represent a statistically small sample set, so any fluid evolution trends are unclear.

The widest calcite array belongs to QUE 99177, plotting along a trend with slope ~0.9. Calcite grains were analyzed from multiple lithologies, including the inter-chondrule matrix and from dark inclusions. Similar to Renazzo, the variation in both $\delta^{18}O$ and $\Delta^{17}O$ (Fig. 1b and b) reflects progressive fluid evolution during aqueous alteration, possibly coupled with mass-dependent fractionation processes.

4.4. Magnetite O isotopes: Orientation effects in SIMS or fluid evolution?

The magnetite O isotopes from CR chondrites do not exhibit the same fractionation trends as the carbonates, and they display distinctly low $\delta^{18}O$ values compared to other chondrite groups (UOC, CV, CI, CM, CK; Rowe et al., 1994; Choi et al., 1998, 2000; Jogo et al., 2011; Davidson et al., 2014; Doyle et al., 2015; Krot and Nagashima, 2016). Magnetite analyses from each meteorite plot along mass-dependent arrays, with no resolvable mass-independent trend (Fig. 6). The lack of variation in $\Delta^{17}O$ (within error) indicates that the magnetite grains did not track O isotopic exchange between fluid and rock within a single meteorite.

The O isotopes for magnetite in GRO 95577,69 show a ~6‰ mass-dependent spread, in contrast to the tightly clustered calcite O isotopes. This spread likely indicates changes in fluid temperature and composition during magnetite formation. The fluid composition may vary along the mass-dependent trend if other minerals (such as carbonates and phyllosilicates) contemporaneously formed from the altering fluid. Similarly, the magnetite O-isotope arrays in Al Rais, Renazzo, EET 92159, and QUE 99177 can be explained in this manner. In Renazzo, the spread in $\delta^{18}O$ is ~10‰, larger than seen in other samples. This is explained by the range in lithologies sampled for Renazzo: dark inclusions, chondrule interiors, and chondrule rims (see Section 4.6 below).

Possible crystal orientation effects in O-isotope measurements of magnetite may complicate interpretations. Single-crystal SIMS analyses of magnetite have been shown to vary in $\delta^{18}O$ between 3 and 6‰. Such variations have been attributed to orientation of the crystal lattice at the time of measurement (Lyon et al., 1998; Huberty et al., 2010; Kita et al., 2011). One possible explanation of this phenomenon is that the secondary ions may be preferentially selected for the light isotope if the crystal planes are near perpendicular to the incident angle of the primary ion beam (Huberty et al., 2010). However, the Hawaii group conducted similar studies on sets of randomly oriented terrestrial magnetite and chromite single-crystals to assess the magnitude of such crystal orientation effects (Caplan et al., 2015). While they found a similar spread of ~3‰ in magnetite, there was no correlation between orientation and the degree of fractionation. Rather, the variations may have reflected differences in crater-bottom roughness that developed during ion probe sputtering, where pitting may have been controlled by the crystal structure.

The cause of the isotope spread of 3 to 6‰ in the CR magnetite grains remains unclear. Efforts to determine the crystal orientation of the magnetite grains in GRO 95577, Al Rais, EET 92159, and QUE 99177 by electron backscatter diffraction (see supplemental material) were inconclusive, potentially because the magnetite grains may not be single-crystals, but rather aggregates of sub-micron crystallites. Questions remain regarding whether or not the SIMS crystal orientation effect and/or crater roughness variations would occur for a series of aggregate crystals. For randomly oriented single-crystal grains, we would theoretically expect to see a spread in the O data reflecting the various orientations. However, for aggregate crystals, we would not expect to see the same 3 to 6‰ spread. According to probability theory and the central limit theorem, a single SIMS measurement that encompasses thousands of randomly oriented sub-micron crystals within an aggregate would represent the convolution of those thousands of crystal orientation effects. Multiple measurements of the aggregate would produce a normal distribution around the expected value, rather than a mass-dependent artifact. Therefore, it seems likely that the variations in O isotopes measured here represent true mass-dependent fractionation trends.

4.5. Models of asteroidal fluid evolution

Interpretations of the progressive alteration trends in O isotopes are highly model-dependent. Progressive alteration

can either shift the O isotopic composition of carbonates toward ^{16}O-enriched or ^{16}O-depleted compositions, depending on the model. The two prevalent schools of thought for asteroidal fluid evolution rely upon the assumption of either open-system or closed-system fluid-rock interaction. Both models can produce the O isotopic compositions observed in carbonaceous chondrites, but with different implications for the alteration process.

Open-system models describe large-scale fluid flow driven by pressure or temperature gradients in the asteroidal parent body (Young et al., 1999; Cohen and Coker, 2000; Young, 2001). Early thermal models predicted that icy planetesimals would have broken up due to vapor overpressure once the ice began to melt (e.g., Grimm and McSween, 1989; Wilson et al., 1999; Young, 2001). By invoking fluid flow, the altering liquid can flow over tens of km on the parent body, releasing water at the surface in the form of vapor and therefore relieving built up pressure. This vapor release and fluid flow over large distances transports water out of the local alteration system.

Open-system models of asteroidal alteration investigate the O isotopic exchange between a heavy water reservoir and a lighter bulk rock in a system experiencing fluid flow (Young et al., 1999; Young, 2001). Such models give rise to a region of intense alteration on the parent body between the center of the asteroid and the frozen outer crust, driven by pressure gradients. In this region, the O compositions of alteration products evolve towards heavier δ^{17}O, δ^{18}O, and higher Δ^{17}O as the alteration process increases, and the fluid flows from high to low temperature (Young et al., 1999; Young, 2001). The O-isotope composition of the rock approaches that of the original water ice as the rock becomes increasingly hydrated by ^{17,18}O-rich fluid. Once the rock is entirely altered, its capacity to exchange O isotopes is exhausted. The altering fluid, now ^{16}O-enriched after exchange with the rock, is partially removed from the body (perhaps ~25% of water ice; Young et al., 1999), and the composition of the planetesimal as a whole becomes ^{16}O-depleted. Rocks further downstream from the interior of the body retain their original ^{16}O-enriched composition and undergo minimal alteration.

The closed-system model also documents the interaction between an ^{17,18}O-enriched fluid and an ^{16}O-enriched anhydrous rock, but comes to a different conclusion (e.g., Clayton and Mayeda, 1984, 1999; Leshin et al., 1997; Benedix et al., 2003; Bland et al., 2009). The main difference between the models is that fluid flow is confined to small scales (~ a few 100 μm) in a closed-system, and water is not lost from the alteration environment. During progressive alteration, the anhydrous rock reacts with water to form secondary minerals, with the dominant alteration products being phyllosilicates (e.g., Weisberg et al., 1993; Brearley, 2006). Phyllosilicates are formed by replacement and hydration of primary silicates, incorporating O isotopes from both the water and the primary rock phases. In the process, the Δ^{17}O of the water decreases as the ^{17,18}O-enriched fluid exchanges O with the ^{16}O-enriched solids. At the same time, equilibrium fractionation will affect the δ^{18}O composition of both the liquids and the new secondary solids (Clayton and Mayeda, 1984; Zheng, 1993). Since no fluid leaves the system, the combined effect causes water to become progressively ^{16}O-enriched as more secondary phases are formed. Through a combination of reaction and exchange, the δ^{17}O, δ^{18}O, and Δ^{17}O of the aqueously formed minerals all decrease during fluid evolution on the parent body (Clayton and Mayeda, 1984, 1999; Leshin et al., 1997; Benedix et al., 2003; Bland et al., 2009).

Many other secondary minerals, such as carbonates and magnetite, precipitate from the altering fluid with the majority of their O isotopes inherited from the aqueous fluid rather than from the primitive rock (e.g., Riciputi et al., 1994). The carbonate and magnetite compositions are fractionated mass-dependently relative to the water, and act as tracers for the fluid composition. The degree of fractionation for each mineral is temperature-dependent, but in general, carbonate minerals are fractionated towards higher δ^{18}O relative to the fluid composition, while magnetite is fractionated towards lower δ^{18}O (Zheng, 1991, 1999; 2011).

Petrographic and compositional observations favor the closed-system model over the open-system model for alteration of CR chondrites. A number of problems exist when considering the open-system model of alteration. The CR chondrites show no evidence for an interconnected network of fractures that would allow for the vigorous fluid flow as described in the open-system models. Veining is rare in CR chondrites, and the few carbonate veins in Renazzo do not extend for regions greater than ~200 μm. Large-scale fluid flow would mobilize and fractionate elements over large distances (over 10's km; Grimm and McSween, 1989; Young et al., 1999; Cohen and Coker, 2000; Bland et al., 2009). Mineralogical maps show that element mobility in CR chondrites is limited to short distances (~ 100 μm) before redeposition (e.g., elements leached from chondrule components are re-precipitated in the surrounding matrix). The bulk elemental compositions of CR chondrites indicate that most CRs are chemically similar (Kallemeyn et al., 1994), with little indication that elements or species were fractionated between meteorite samples. Further evidence for isochemical alteration in CR chondrites lies in the nearly identical elemental compositions of the hydrated matrix from Renazzo compared to the primitive matrices of QUE 99177 and MET 00426 (Zolensky et al., 1993; Jilly and Huss, 2012). The O isotopic compositions for minerals in the most heavily altered CR chondrite GRO 95577 can also clarify the direction of fluid evolution. The GRO 95577 magnetite compositions fall near the ^{16}O-enriched end of the mass-independent O isotope trend (Figs. 1 and 6), indicating that the water was enriched in ^{16}O after progressive alteration.

The open-system models also neglect to account for the observed sub-micron grain size of the matrix material. The open-system models assume that the fine-grained matrix is analogous in permeability and porosity to Lunar soils (Grimm and McSween, 1989; Young et al., 1999; Cohen and Coker, 2000; Young, 2001). Bland et al. (2009) revised estimates for grain- and pore-size distributions to more accurately reflect primitive chondrite matrices, which decreased the modeled permeability of the rock and restricted the flow of water on the parent body. Under these

revised conditions, thermal models more closely reflect the chemical observations of chondrite samples, and suggest that alteration occurred in a closed-system with small length-scales of liquid water transport (Clayton and Mayeda, 1984, 1999; Benedix et al., 2003; Bland et al., 2009).

4.6. Lithologies and mineral contributions to the CR whole-rock mixing line

The whole-rock O-isotope trend for CR chondrites (Fig. 1) is generally interpreted as a progressive alteration trend, representing a two-component mixture between an ^{16}O-enriched solid reservoir, and an ^{17,18}O-enriched H_2O reservoir (Clayton and Mayeda, 1984, 1999; Rowe et al., 1994; Young et al., 1999; Schrader et al., 2011). However, there are some fine-scale inconsistencies, particularly for the more heavily altered samples, where the relative position in the progressive alteration trend is inconsistent with the petrologic type (Schrader et al., 2011, 2014a). What complicates this issue is that progressive alteration trends for the bulk rock are different than trends for some individual secondary minerals. As explained in Section 4.5 above, calcite and magnetite compositions follow the fluid evolution. As the bulk rock becomes ^{17,18}O-enriched during alteration, the fluid (and magnetite and calcite) compositions become progressively ^{16}O-enriched. Understanding the behavior of O isotopes in individual minerals (such as carbonate and magnetite) may therefore help to determine the source of the bulk rock inconsistencies.

In the context of the closed-system model of progressive alteration (Clayton and Mayeda, 1984, 1999; Leshin et al., 1997; Benedix et al., 2003; Bland et al., 2009), the carbonate and magnetite O isotopes should theoretically display a progressive alteration trend that correlates with the petrologic type. For example, the magnetites and carbonates from QUE 99177 (the least altered CR) would be expected to be depleted in ^{16}O relative to those in GRO 95577 (extremely altered CR), and the remaining samples would fall in between the two extremes (e.g., Benedix et al., 2003). Surprisingly, the compositions of secondary minerals measured *in situ* do not demonstrate a correlation between composition and petrologic type (Fig. 7a, referencing the petrologic type scheme of Harju et al., 2014). For example, the CRs of lowest petrologic type in this study, GRO 95577 and Al Rais (Alexander et al., 2013; Harju et al., 2014; Howard et al., 2015), plot at the lightest and heaviest ends of the magnetite trend. All higher petrologic types plot between these two heavily altered samples.

The lack of correlation between the petrologic type and the mineral O isotopes suggests that either the simple two-component hydration model is not sufficient to explain the progressive alteration of CR chondrites, or the petrologic type characterizations do not adequately represent the specimens. As mentioned previously, numerous methods for classifying the CR petrologic types have recently been proposed (Alexander et al., 2013; Harju et al., 2014; Schrader et al., 2014a; Howard et al., 2015; Abreu, 2016), but no scheme can fully account for the complex variations in clast, component, and dark inclusion abundances across the CR spectrum.

To understand why secondary mineral compositions do not correlate with petrologic type, we analyzed the calcite and magnetite O isotopes in terms of their lithologies. We categorized the main lithologic components of CR chondrites to be metal-rich chondrules, fine-grained matrix, fine-grained chondrule rims, and dark inclusions. We have measured magnetite and carbonates from each of these lithologies across the different samples. When plotted as a function of lithology, an interesting pattern emerges for the magnetite grains. The different lithologies plot in distinct clusters on the three O-isotope diagram. In order of increasing ^{16}O-enrichment (toward the lower left of the diagram), they define the following order: matrices, chondrule rims, dark inclusions, chondrule interiors (Fig. 7b). This pattern is exemplified in Renazzo where we measured magnetite from multiple dark inclusions, a chondrule interior, and a chondrule rim. Magnetite from each different Renazzo lithology plots near similar lithologies from other CR chondrite samples.

This trend indicates an order of formation from an evolving fluid in the context of the closed-system progressive alteration model. The *in situ* O isotopes reveal that magnetite in the matrix formed first, followed by that in fine-grained chondrule rims, then the magnetite in dark inclusions, and then that in chondrule interiors. This progressive alteration trend is supported by petrographic evidence that the matrix is the first material to become altered, and that the alteration of chondrule interior metal occurs during more advanced states of alteration (Weisberg et al., 1993; Brearley, 2006; Abreu and Brearley, 2010). While metal can be oxidized quickly by water, Fe,Ni-metal nodules on the interiors of chondrules are often protected by the robust surrounding silicate phenocrysts. In this scenario, the fluid evolution is dominated by phyllosilicate formation, which progressively shifts the fluid toward a lighter O composition (e.g., Choi et al., 1998). The reverse trend would be expected if magnetite were the only mineral forming from the fluid, since magnetite O isotopes are fractionated towards lower δ^{18}O relative to the composition of the fluid. Petrographic observations support the assumption that phyllosilicate formation dominates the aqueous alteration process. Phyllosilicates and clays are formed throughout all stages of alteration; first they form during the alteration of fine-grained matrices and chondrule mesostasis, and later during the alteration of chondrule silicates (Weisberg et al., 1993; Brearley, 2006; Abreu and Brearley, 2010).

The calcite lithologies do not show the same trend as the magnetite (Fig. 7b). Rather, the matrix carbonates track fluid evolution. The large spread in matrix calcites may indicate a prolonged period of carbonate formation, with continual precipitation in the fine-grained lithology as the fluid evolved.

The spread in O isotopes for matrix calcites may also reflect the varying W/R ratios for each meteorite. In terms of mass-balance, the amplitude of δ^{18}O isotopic evolution in minerals would be less in a water-rich system than in a system with low W/R ratio (Agrinier and Cannat, 1997).

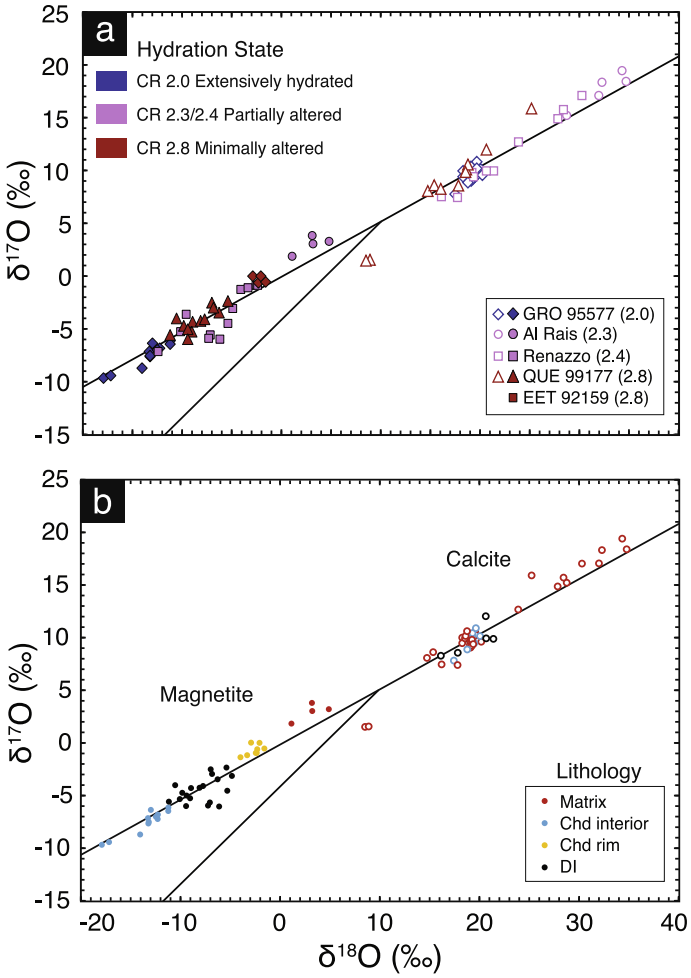

Fig. 7. (a) Secondary calcite (open symbols) and magnetite (closed symbols) O isotopes arranged by the petrologic type designation of Harju et al. (2014). Sample data points are color-coded by the degree of alteration, ranging from heavily hydrated (blue) to minimally altered (red). There is no correlation between the O isotope trend and petrologic type. (b) Secondary calcite (open symbols) and magnetite (closed symbols) O isotopes arranged by lithology. Uncertainties and dolomite analyses have been removed for clarity.

Quantitative estimates of W/R ratios in CR chondrite samples (e.g., Clayton and Mayeda, 1999; Schrader et al., 2011) have recently been shown to be invalid for CR chondrites (Schrader et al., 2014a). The W/R models require assumptions about the homogeneity of the matrix and the bulk anhydrous O compositions that do not apply to the lithologically and isotopically heterogeneous CRs (Schrader et al., 2014a). Although there are no valid estimates of the absolute W/R ratios, less altered samples have, in general, relatively lower W/R ratios than heavily altered samples (Clayton and Mayeda, 1999). We therefore compared the degree of alteration to the extent of fluid evolution for each matrix calcite trend. The extent of fluid evolution is quantified by the spread in measured $\delta^{18}O$ and $\Delta^{17}O$ for a given meteorite. Our analyses follow the predicted correlation; the matrix calcites in heavily hydrated (high W/R) samples show smaller degrees of fluid evolution than less-altered (low W/R) samples (Fig. 8). In terms of increasing $\delta^{18}O$ isotopic evolution, GRO 95577 < Al Rais < Renazzo < QUE 99177, consistent with the petrologic type schemes of Harju et al. (2014) and Howard et al. (2015). A similar trend is apparent for $\Delta^{17}O$, but the uncertainty in $\Delta^{17}O$ is too large to distinguish small variations at high W/R ratios. This data suggests that the extent of local fluid evolution may be controlled by the W/R ratio. Some possible causes of local variations in W/R could include heterogeneous distribution of ice during parent-body accretion, radial location in the parent body, variable porosity and/or permeability (e.g., Alexander et al., 2013), or short-lived external heating of ice via impacts.

When comparing the different trends for calcite and magnetite O isotopes, the magnetite appears to have been formed under a more limited set of fluid conditions. One possible explanation may be variations in fluid chemistry during alteration. In CR chondrites, Fe is primarily sequestered in Fe-metal (and some sulfides), and is rapidly oxidized to magnetite upon interaction with water. Once the metal is exhausted, magnetite may cease, and instead Fe-bearing phyllosilicates form as replacement products for primary silicates. It is possible in more heavily altered CRs that magnetite may form later from Fe released by early-formed Fe-rich phyllosilicates, or from alteration of

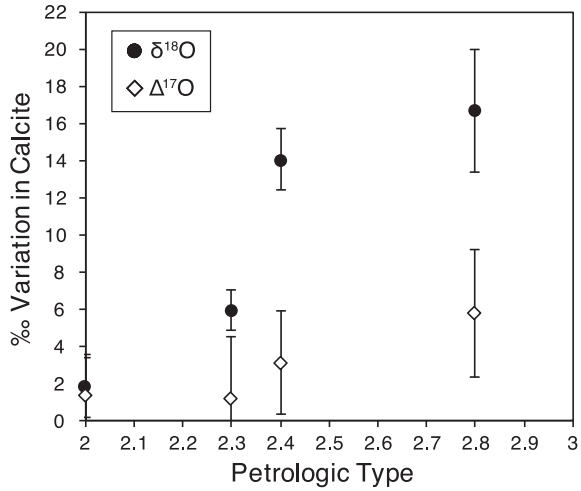

Fig. 8. Graph depicting the variation of O isotopes for matrix calcite (‰) versus the petrologic type (Harju et al., 2014) for four CR chondrites: GRO 95577 (2.0), Al Rais (2.3), Renazzo (2.4), QUE 99177 (2.8). This plot shows correlations between $\delta^{18}O$ or $\Delta^{17}O$ and the relative degree of alteration. The data for $\Delta^{17}O$ is less conclusive due to the smaller fractionations and large uncertainties in the analyses. Error bars are 2σ.

Fe-sulfides (Zolensky et al., 1997; Howard et al., 2015); however, the majority of magnetite is thought to form early from oxidation of Fe-metal (e.g., Kallemeyn et al., 1994). In contrast, Ca is sequestered in multiple minerals with variable dissolution rates. As long as there is a source of C (such as CO_2, organics, or poorly graphitized C), calcite may form at the initial stages of alteration as Ca is leached from the glassy mesostasis, through the final stages of alteration when Ca is dissolved into the fluid during the replacement of pyroxene crystals. Other Ca-bearing secondary phases in CR chondrites such as phosphates and smectites may also form, but require additional cations in the solution and must overcome higher energy barriers to begin nucleation.

It should be noted that the accuracy of these observed lithologic patterns are limited by the extreme heterogeneity of CR chondrites. For instance, not all magnetite and carbonate-containing lithologies were found in each sample. Carbonates from fine-grained rims were not large enough to be measured by SIMS, no magnetite grains were measured from dark inclusions in GRO 95577, and the only matrix magnetites measured here were from Al Rais. While the trends pointed out here suggest interesting formation patterns, larger-scale studies would be necessary to eliminate concerns about sample bias. Furthermore, magnetite isotopes from a petrographically unique dark inclusion in Renazzo (Fig. 9) plot at slightly low $\Delta^{17}O$ (ranging from −2.0 to –2.9‰, close to the anomalous magnetite in MIL 090292 (ranging from −2.5 to –4.4‰). This variation may support the idea that some dark inclusions (but not all) have an exogenous origin (Endreß et al., 1994). However, no carbonates were measured in this unique clast, so a more thorough study would be needed to determine its origin.

The inconsistencies in the whole-rock trend can be explained by lithologic heterogeneity and fluid evolution. Particularly for the most altered samples, fluid evolution will drag the isotopic composition of secondary minerals towards a lighter O composition, in the opposite direction of the simple two-component whole-rock mixing line. Abundant ^{18}O-poor magnetite in GRO 95577 may pull the bulk composition towards the less-altered end of the CR trend, while the ^{18}O-rich matrix magnetite and calcite in Al Rais shift the bulk values towards the altered end of

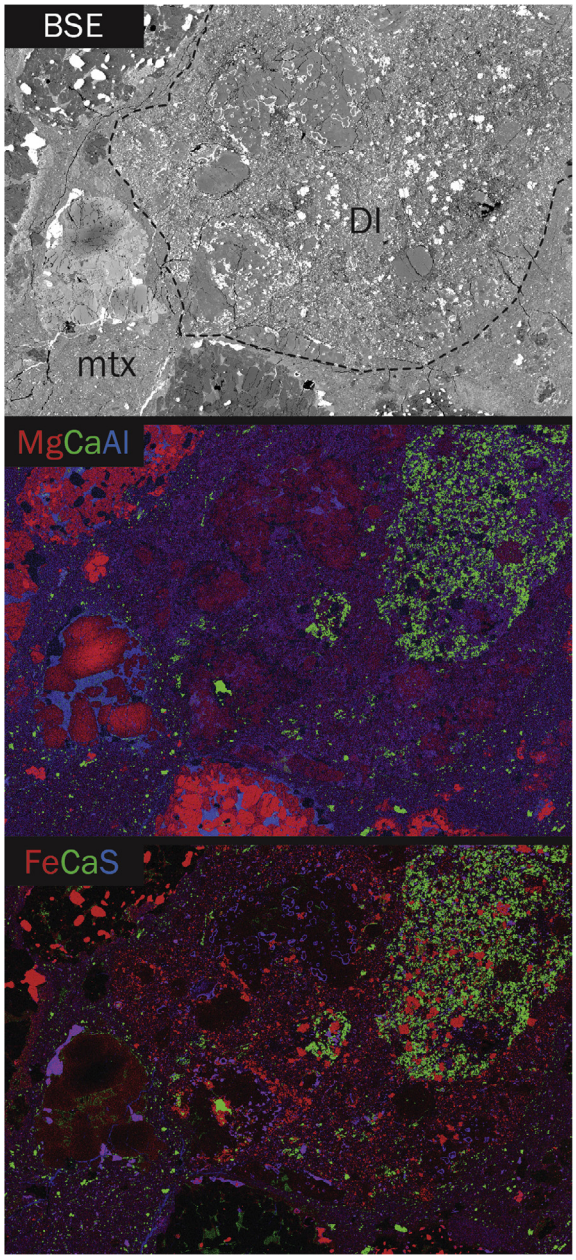

Fig. 9. Unique dark inclusion (DI) in Renazzo N1126. This inclusion contains abundant magnetite and calcite, but the crystal habits are tabular and dissimilar to other DI clasts. This DI also contains a region rich in Ca-Fe silicate material (possibly Kirschteinite).

the CR mixing trend. Since the O isotopic compositions appear to vary by lithology, our data support the idea that not all clasts were altered *in situ*, but that some were incorporated as pre-altered lithologies from elsewhere on the CR parent body (or possibly from an exogenous source), complicating the whole-rock signature. This research supports the findings of Abreu (2016), that defining quantitative petrologic types for CR chondrites would require a multi-technique approach due to their complex history and lithological diversity. Alternatively, a new petrologic type scheme could be developed that classifies clasts or lithologies rather than the meteorite as a whole, as is done with complex breccias such as the Kaidun meteorite.

4.7. Oxygen isotope geothermometry and fluid evolution

The relative O-isotope fractionation between carbonate and magnetite can be used as a geothermometer for aqueous alteration (Zheng, 1991; Choi et al., 2000; Zheng, 2011). Fractionation factors have been empirically derived for calcite-water (Eq. (3); Zheng, 2011), dolomite-water (Eq. (4); Zheng, 2011) and magnetite-water (Eq. (5); Zheng, 1991) systems at low temperatures, where T = temperature (in K), and $\alpha = [(^{18}O/^{16}O)_{mineral} / (^{18}O/^{16}O)_{water}]$.

$$\text{Calcite-water}: 10^3 \ln\alpha = 4.01 \times 10^6/T^2 - 4.66 \times 10^3/T + 1.71 \quad (3)$$

$$\text{Dolomite-water}: 10^3 \ln\alpha = 4.06 \times 10^6/T^2 - 4.65 \times 10^3/T + 1.71 \quad (4)$$

$$\text{Magnetite-water}: 10^3 \ln\alpha = 3.02 \times 10^6/T^2 - 12.00 \times 10^3/T + 3.31 \quad (5)$$

At temperatures of interest for minimally-metamorphosed chondrites (<~400 °C), the magnetite and calcite fractionation curves show different trends (Fig. 10). In calcite, O isotopes are fractionated towards positive values relative to water. Fractionation is greatest at near-freezing temperatures, and exponentially decreases with rising temperature. By ~500 °C, the fractionation factor has plateaued near zero (Zheng, 2011). The dolomite O partitioning curve is nearly identical to calcite, with ~+1‰ offset near 0 °C, so it is not plotted in Fig. 10 for clarity. For magnetite, the O is fractionated towards negative values between 0 and 500 °C. The fractionation curve reaches a minimum of $10^3 \ln\alpha \sim -8$ near 225 °C, then gradually approaches $10^3 \ln\alpha = 0$ at higher temperatures (Zheng, 1991).

To extract temperature information from a single mineral composition, the fluid composition must be known. In the case that two minerals are formed at the same time from a uniform fluid, the relative equilibrium-fractionation factors can provide temperature information without knowledge of the water composition (Chiba et al., 1989; Choi et al., 2000). While it is petrographically difficult to determine equilibrium assemblages for such sedimentary matrix material, we assume that local fluid equilibrium and co-precipitation is valid if the following criteria are met: 1. The two secondary minerals must occur in the same clast/lithology. 2. The minerals should be associated or frequently in contact, but with no evidence that one was clearly formed before the other. 3. The minerals lie on the same mass-dependent fractionation line (indistinguishable $\Delta^{17}O$ values), consistent with formation in equilibrium from a common reservoir (Clayton and Mayeda, 1984, 1999; Choi et al., 2000).

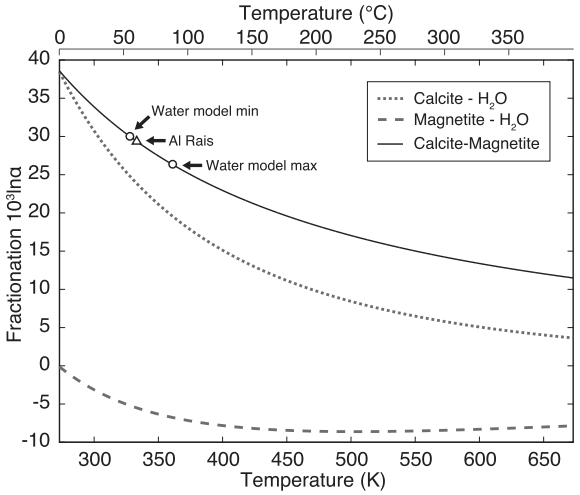

Fig. 10. Diagram of fractionation curves for precipitation of magnetite and calcite from an aqueous solution at varying temperature. The degree of fractionation is given in units of $10^3 \ln(\alpha)$, where $\alpha = [(^{18}O/^{16}O)_{mineral}/(^{18}O/^{16}O)_{water}]$. The magnetite-water curve is shown as a dashed line (Zheng, 1991) and the calcite-water curve as a dotted line (Zheng, 2011). The dolomite-water curve is not shown, as it is nearly identical to the calcite-water curve. The solid black line represents the relative fractionation between calcite and magnetite. If produced from a fluid in local thermodynamic equilibrium, calcite-magnetite assemblage in Al Rais was formed at ~60 °C. Al Rais data used for calculations correspond to grains C01 and M02 in Tables 2 and 4, respectively. Minimum and maximum temperatures from a global CR parent body water evolution model are also shown (see text).

Since the composition of water on the CR parent body is unknown or poorly constrained (e.g., Clayton and Mayeda, 1999; Schrader et al., 2011, 2013, 2014b), the calcite-magnetite and dolomite-magnetite fractionations can provide insight into both the temperature and water composition at the time of alteration. The black solid line in Fig. 10 represents the relative fractionation between calcite and magnetite precipitated from a uniform fluid at varying temperatures (Eq. (6)). The dolomite and magnetite fractionation curve is nearly identical (Eq. (7)).

$$\text{Calcite-magnetite}: 10^3 \ln\alpha = 0.99 \times 10^6/T^2 + 7.34 \times 10^3/T - 1.60 \quad (6)$$

$$\text{Dolomite-magnetite}: 10^3 \ln\alpha = 1.04 \times 10^6/T^2 + 7.35 \times 10^3/T - 1.60 \quad (7)$$

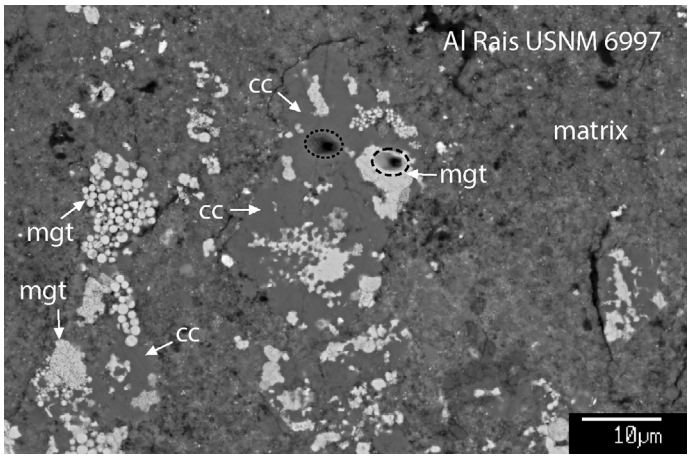

Fig. 11. BSE image of a calcite (cc) and magnetite (mgt) assemblage in Al Rais. Ion probe pits are indicated by dotted (cc) and dashed (mgt) circles. The calcite analysis corresponds to Al Rais grain C01 in Table 2, and the magnetite analysis corresponds to Al Rais grain M02 in Table 4.

A characteristic carbonate-magnetite assemblage in Al Rais USNM 6997 (Fig. 11) is a good candidate for co-precipitation. This assemblage contains abundant magnetite spherules and framboids, intergrown with calcite. Both minerals were measured for O isotopes, yielding a relative fractionation of 29.9 ± 2.2‰ along a mass-dependent fractionation line ($\Delta^{17}O \sim 1‰$; Fig. 1). This large fractionation implies a formation temperature of 60 ± 19 °C (Fig. 10); the uncertainties are 2σ contributions from O isotopes, but do not include uncertainties from the fractionation model. Fractionation factors determined by the models are stated to be within ±5% of the empirical factor values (Zheng, 1991, 2011). If we incorporate model uncertainty for a more conservative error estimate, the uncertainty in temperature would be ±22 °C. The temperature and fractionation factors for this equilibrium assemblage in Al Rais would require a fluid with O isotopic composition of $\Delta^{17}O \sim 1‰$ and $\delta^{18}O \sim 10‰$. This alteration temperature is on the low-end of previously estimated temperatures for CR chondrites (50 to 150 °C; Zolensky et al., 1993; <240 °C; Busemann et al., 2007; 0 to 171 °C; Cody et al., 2008), but is similar to some estimated temperatures for CM and CO chondrite alteration (e.g., Clayton and Mayeda, 1984, 1999; Zolensky et al., 1993; Brearley, 2006; Guo and Eiler, 2007; Verdier-Paoletti et al., 2017).

If the assumption is true that all lithologies measured here come from a single CR parent body altered in a closed system, then all data from a single mineral may be interpreted as a progressive alteration trend. Each trend (one for calcite, one for magnetite) shows how the O composition of that mineral varied during fluid evolution. The regression through all calcite data yields a slope of 0.64 ± 0.04, and the regression through the magnetite data (not including MIL 090292) yields a similar slope of 0.63 ± 0.05 (Figs. 1 and 12). The 2σ uncertainties suggest that these trends are distinct from mass-dependent slope-0.52 trends, and that the calcite and magnetite minerals reflect statistically identical fluid evolution trends. In the case that both trends reflect fractionation from a phyllosilicate-dominated fluid evolution on the CR parent body, then some inferences about the average temperature and O composition during fluid evolution can be made. The relative $\delta^{18}O$ fractionation between the calcite and magnetite trends for each $\Delta^{17}O$ value yields a range of average "global" temperature during CR parent body alteration of ~55 to 88 °C (Fig. 10). The matrix phases in Al Rais would have represented some of the earliest stages of alteration of CR chondrites. Subsequent alteration would cause the fluid composition to become increasingly ^{16}O-enriched, following a similar slope-0.63 line as the magnetite and calcite trends, ending near a final fluid composition of $\Delta^{17}O \sim -1.2‰$ and $\delta^{18}O \sim -15‰$ (Fig. 12). While this interpretation is likely a simplification of many combined processes, it provides a first-order estimate of both the composition and evolution of fluid on the CR parent body.

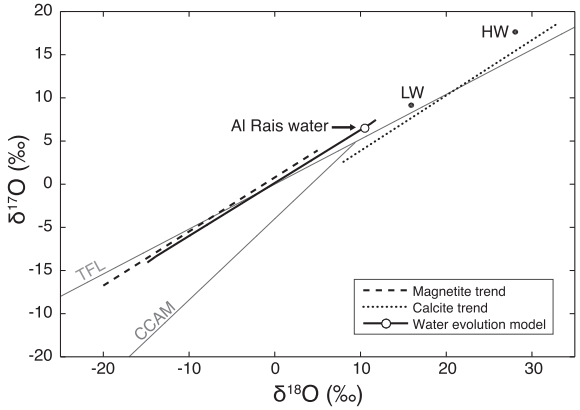

Fig. 12. Model for the evolution of CR water during progressive alteration. Depicted are the O isotope trends for magnetite (dashed line), and calcite (dotted line). Also on the plot are the compositions of the light (LW) and heavy (HW) water compositions from Clayton and Mayeda (1999). We show that the CR water evolved from near the composition labeled "Al Rais water", down toward ^{16}O-enriched values along the water evolution model (solid line).

The fluid evolution was influenced to some extent by O isotopic exchange between the anhydrous solids and the fluid, most likely due to the formation of phyllosilicates. The O isotopic composition of the anhydrous CR solids is predominantly controlled by abundant type-I-chondrule silicates, which have typical $\Delta^{17}O$ values ranging from ~ -6 to 0‰ (Krot et al., 2006; Connolly and Huss, 2010; Schrader et al., 2013, 2014b, 2017; Tenner et al., 2015). QUE 99177, considered to be the least hydrated CR chondrite, has bulk $\Delta^{17}O = -2.89 \pm 0.06$ (Schrader et al., 2011, 2014a). While silicates from relict grains and CAIs can have $\Delta^{17}O$ compositions down to ~−25‰, these grains are relatively rare, and therefore do not control the bulk solid O composition available for O isotope exchange. Since the majority of CR anhydrous solids do not have extreme $\Delta^{17}O$ values, the slope of these alteration trends would not vary by large amounts even if O isotope exchange was substantial. The small variation in secondary mineral $\Delta^{17}O$ and low-temperature alteration does not support a highly $^{17,18}O$-enriched ice reservoir, such as in UOCs ($\delta^{18}O = 21‰$, $\Delta^{17}O \sim 7‰$; Choi et al., 1998) or the heavy hater (HW) proposed for CI and CM chondrites ($\delta^{18}O = 28.1‰$, $\delta^{17}O = 17.7‰$, $\Delta^{17}O = 3.1‰$; Clayton and Mayeda, 1999). The CR water–ice reservoir instead likely had values closer to $\delta^{18}O \sim 11‰$, $\delta^{17}O \sim 7‰$, and $\Delta^{17}O \sim 2‰$ to yield the carbonate and magnetite compositions observed here, consistent with estimates from other studies of CR chondrites ($\Delta^{17}O \sim 0$ to 5‰; Schrader et al., 2014a, b; Tenner et al., 2015).

5. CONCLUSIONS

We successfully measured *in situ* O isotopes for secondary calcite, dolomite, and magnetite in a variety of lithologies for six CR chondrites of different petrologic type. In this study, we find:

1. Calcite O isotopes are generally fractionated toward positive $\delta^{18}O$ relative to SMOW. All calcite grains form a general trend with a slope of ~0.64 near the TFL. Individually, the compositions of calcite grains in the host matrices of each CR chondrite track fluid evolution. The extent of evolution correlates with the degree of alteration, suggesting that O isotope evolution was more rapid in samples with a lower W/R ratio, such as QUE 99177. The extensively hydrated GRO 95577 experienced little to no fluid evolution during carbonate precipitation, reflecting the high W/R ratio of the sample. A variety of W/R ratios in CR samples supports the idea that aqueous alteration was spatially heterogeneous, with some regions potentially accreting more water–ice than others.
2. Magnetite O isotopes are generally fractionated toward negative $\delta^{18}O$ relative to SMOW. All magnetite grains (excluding MIL 090292) form a general trend with a slope of ~0.63 near the TFL. On an individual basis, magnetite compositions show that distinct lithologies may record various stages in the alteration process, consistent with models of progressive alteration. Similar progressive alteration trends have been applied to whole-rock O isotopes, but do not hold up for the most altered samples due to the complex heterogeneity of CR chondrites and the extreme variation in component abundances.
3. MIL 090292 either has an anomalous origin, or is not a CR chondrite. Magnetite O isotopes from MIL 090292,12 fall off of the general trend for other CR chondrites. The secondary mineralogy is different than typical CR chondrites, with no evidence of Ca-carbonates. Instead, Ca resides in secondary Ca-silicates, such as Ca-pyroxene, hedenbergite, and andradite.
4. The isotopic compositions of secondary minerals do not correlate with existing petrologic type classifications for each CR chondrite. This observation can explain inconsistencies in whole-rock O isotopic progressive alteration trends. For example, the high abundance of ^{16}O-depleted magnetite and calcite in Al Rais as compared to ^{16}O-enriched compositions in GRO 95577 can shift the bulk isotopic compositions away from the theoretical bulk-rock alteration trends.
5. The alteration temperature estimated for a calcite-magnetite assemblage in Al Rais is ~60 °C, with a fluid composition of $\Delta^{17}O \sim 1‰$ and $\delta^{18}O \sim 10‰$. The calcite and magnetite CR trends suggest that aqueous alteration temperatures on the CR parent body globally ranged from ~55 to 88 °C. The matrix phases in Al Rais represent some of the earliest stages of alteration of CR chondrites; subsequent alteration caused the fluid to evolve along a slope-0.63 line, with final fluid composition of $\Delta^{17}O \sim -1.2‰$ and $\delta^{18}O \sim -15‰$. The unique O compositions of secondary minerals in CR chondrites suggest a water reservoir with a composition near $\Delta^{17}O \sim 2‰$, different than the heavy water compositions proposed for UOC (Choi et al., 1998), CM and CI (Clayton and Mayeda, 1999) chondrites.

ACKNOWLEDGEMENTS

We thank the Johnson Space Center's Meteorite Working Group for the Antarctic meteorite samples, and the Division of Meteorites, Department of Mineral Sciences, Smithsonian Institution for providing the Al Rais USNM 6997 samples. We also thank the Museum of Natural History Vienna for providing the Renazzo NHMW-N1126 and NHMW-N1127 samples. The authors also thank N. Kita for insight on magnetite fractionation, and M. Garcia for sharing his writing knowledge. This manuscript was improved by the helpful reviews from T. Tenner and two anonymous reviewers, and Associate Editor S. Russell. This work was supported by NASA Headquarters under the NASA Earth and Space Science Fellowship Program – Grant NNX14AO29H, as well as NASA Cosmochemistry Grant NNX11AG78G (G. R. Huss, PI), and NAI cooperative agreement NNA04CC08A (K. Meech, PI). This manuscript is SOEST publication #10235 and HIGP publication #2262.

APPENDIX A. SUPPLEMENTARY MATERIAL

Supplementary data associated with this article can be found, in the online version, at https://doi.org/10.1016/j.gca.2017.10.007.

REFERENCES

Abreu N. M. (2015) Processes affecting the CR chondrites parent body: Petrology, mineralogy and chemical composition of the matrices of Antarctic CR carbonaceous chondrites. *Lunar Planet. Sci. Con. XLVI,* #2561.

Abreu N. M. (2016) Why is it so difficult to classify Renazzo-type (CR) carbonaceous chondrites? Implications from TEM observations of matrices for the sequences of aqueous alteration. *Geochim. Cosmochim. Acta* **194**, 91–122.

Abreu N. M. and Brearley A. J. (2005) Carbonates in Vigarano: Terrestrial, preterrestrial, or both? *Meteorit. Planet. Sci.* **40**, 609–625.

Abreu N. M. and Brearley A. J. (2010) Early solar system processes recorded in the matrices of two highly pristine CR3 carbonaceous chondrites, MET 00426 and QUE 99177. *Geochim. Cosmochim. Acta* **74**, 1146–1171.

Aharon P. (1988) O, carbon and U-series isotopes of aragonites from Vesfold Hills, Antarctica: Clues to geochemical processes in subglacial environments. *Geochim. Cosmochim. Acta* **52**, 2321–2331.

Alexander C. M. O. D., Bowden R., Fogel ML., Howard KT., Herd CDK. and Nittler LR. (2012) The provenances of asteroids, and their contributions to the volatile inventories of the terrestrial planets. *Science* **337**, 721–723.

Alexander C. M. O. D., Howard KT., Bowden R. and Fogel ML. (2013) The classification of CM and CR chondrites using bulk H, C, and N abundances and isotopic compositions. *Geochim. Cosmochim. Acta* **123**, 244–260.

Agrinier P. and Cannat M. (1997) O-isotope constraints on serpentinization processes in ultramafic rocks from the Mid-Atlantic Ridge (23°N). In *Proceedings of the Ocean Drilling Program, Scientific Results* **153**. College Station, TX. pp. 381–388.

Baertschi P. (1976) Absolute ^{18}O content of standard mean ocean water. *Earth Planet. Sci. Lett.* **31**, 341–344.

Benedix G. K., Leshin L. A., Farquhar J., Jackson T. and Thiemens M. H. (2003) Carbonates in CM2 chondrites: Constraints on alteration conditions from O isotopic compositions and petrographic observations. *Geochim. Cosmochim. Acta* **67**, 1577–1588.

Bland P. A., Sexton A., Jull A. J. T., Bevan A. W. R., Berry F. J., Thornley D., Astin T. and Pillinger C. T. (1998) Climate and rock weathering: A study of terrestrial age dated ordinary chondritic meteorites from hot desert regions. *Geochim. Cosmochim. Acta* **62**, 3169–3184.

Bland P. A., Lee M. R., Sexton A. S., Franchi I. A., Fallick A. E. T., Miller M. F., Cadogan J. M., Berry F. J. and Pillinger C. T. (2000) Aqueous alteration without a pronounced oxygen-isotopic shift: Implications for the asteroidal processing of chondritic materials. *Meteorit. Planet. Sci.* **35**, 1387–1395.

Bland P.A., Zolensky M. E., Benedix G.E., and Sephton M.A. (2006) Weathering of Chondritic Meteorites. In *Meteorites and the Early Solar System II* (eds. Lauretta D. S. and McSween H. Y.). pp. 853–867.

Bland P. A., Jackson M. D., Coker R. F., Cohen B. A., Webber J. B. W., Lee M. R., Duffy C. M., Chater R. J., Ardakani M. G., McPhail D. S., McCombb D. W. and Benedix G. K. (2009) Why aqueous alteration in asteroids was isochemical: High porosity ≠ high permeability. *Earth Planet. Sci. Lett.* **287**, 559–568.

Brearley A. J. (2006) The action of water. In *Meteorites and the Early Solar System II* (eds. Lauretta D. S. and McSween H. Y.), pp. 584–624.

Busemann H., Alexander C. M. O. D. and Nittler L. (2007) Characterization on insoluble organic matter in primitive meteorites by microRaman spectroscopy. *Meteorit. Planet. Sci.* **42**, 1387–1416.

Caplan C. E., Huss G. R., Hammer J. E., Ogliore R. C., and Nagashima K. (2015) Crystal orientation effects for oxygen-isotope measurements of magnetite and chromite. *Ann. Meteorit. Soc. Meet.* #5333.

Cassidy W., Harvey R., Schutt J., Delisle G. and Yanai K. (1992) The meteorite collection sites of Antarctica. *Meteoritics* **27**, 490–525.

Chiba H., Chacko T., Clayton R. N. and Goldsmith J. R. (1989) O isotope fractionations involving diopside, forsterite, magnetite, and calcite: Application to geothermometry. *Geochim. Cosmochim. Acta* **53**, 2985–2995.

Choi B.-G. and Wasson J. T. (2003) Microscale O isotopic exchange and formation of magnetite in the Ningqiang anomalous carbonaceous chondrite. *Geochim. Cosmochim. Acta* **67**, 4655–4660.

Choi B.-G., McKeegan K. D., Leshin L. A. and Wasson J. T. (1997) Origin of the magnetite in oxidized CV chondrites: In situ measurement of O isotopic compositions of Allende magnetite and olivine. *Earth Planet. Sci. Lett.* **146**, 337–349.

Choi B.-G., McKeegan K. D., Krot A. N. and Wasson J. T. (1998) Extreme O-isotope compositions in magnetite from unequilibrated ordinary chondrites. *Nature* **392**, 577–579.

Choi B.-G., Krot A. N. and Wasson J. T. (2000) O isotopes in magnetite and fayalite in CV chondrites Kaba and Mokoia. *Meteorit. Planet. Sci.* **35**, 1239–1248.

Choi B.-G., Ahn I., Ziegler K., Wasson J. T., Young E. D. and Rubin A. E. (2009) O isotopic compositions and degree of alteration of CR chondrites. *Meteorit. Planet. Sci.* **44**, A50.

Clayton R. N. and Mayeda T. K. (1984) The O isotope record in Murchison and other carbonaceous chondrites. *Earth Planet. Sci. Lett.* **67**, 151–161.

Clayton R. N. and Mayeda T. K. (1999) O isotope studies of carbonaceous chondrites. *Geochim. Cosmochim. Acta* **63**, 2089–2104.

Cody G. D., Alexander C. M. O'D., Yabuta H., Kilcoyne A. L. D., Araki T., Ade H., Dera P., Fogel M., Militzar B. and Mysen B. O. (2008) Organic thermometry for chondritic parent bodies. *Earth Planet. Sci. Lett.* **272**, 446–455.

Cohen B. A. and Coker R. F. (2000) Modeling of liquid water on CM meteorite parent bodies and implications for amino acid racemization. *Icarus* **145**, 369–381.

Connolly H. C. and Huss G. R. (2010) Compositional evolution of the protoplanetary disk: Oxygen isotopes of type-II chondrules from CR2 chondrites. *Geochim. Cosmochim. Acta* **74**, 2473–2483.

Davidson J., Krot A. N., Nagashima K., Hellebrand E. and Lauretta D. S. (2014) O isotope and chemical compositions of magnetite and olivine in the anomalous CK3 Watson 002 and ungrouped Asuka-881595 carbonaceous chondrites: Effects of parent body metamorphism. *Meteorit. Planet. Sci.* **49**, 1456–1474.

Doyle P. M., Jogo K., Nagashima K., Krot A. N., Wakita S., Ciesla F. J. and Hutcheon I. D. (2015) Early aqueous activity on the chondrite parent asteroids recorded by fayalite. *Nat. Comm.* **6**, 1–10.

Endreß M., Keil K., Bischoff A., Spettel B., Clayton R. N. and Mayeda T. K. (1994) Origin of dark clasts in the Acfer 059/El Djouf 001 CR2 chondrite. *Meteoritics* **29**, 26–40.

Fahey A. J., Goswami J. N., McKeegan K. D. and Zinner E. K. (1987) ^{16}O excesses in Murchison and Murray hibonites: A case against late supernova injection origin of isotopic anomalies in O, MG, Ca, and Ti. *Astrophys. J. Lett.* **323**, L91–L95.

Faure G., Hoefs J., Jones L. M., Curtis J. B. and Pride D. E. (1988) Extreme ^{18}O depletion in calcite and chert clasts from the

Elephant Moraine on the East Antarctic ice sheet. *Nature* **332**, 352–354.

Gooding J. L. (1986) Weathering of stony meteorites in Antarctica. *Int. Workshop Antarct. Meteorites* **1**, 48–54.

Grimm R. E. and McSween H. Y. (1989) Water and the thermal evolution of carbonaceous chondrite parent bodies. *Icarus* **82**, 244–280.

Guo W. and Eiler J. M. (2007) Temperatures of aqueous alteration and evidence for methane generation on the parent bodies of the CM chondrites. *Geochim. Cosmochim. Acta* **71**, 5565–5575.

Hanshaw B. B. and Hallet B. (1978) O isotope composition of subglacially precipitated calcite: possible paleoclimatic implications. *Science* **200**, 1267–1270.

Hays P. D. and Grossman E. L. (1991) O isotopes in meteoric calcite cements as indicators of continental paleoclimate. *Geology* **19**, 441–444.

Harju E. R., and Rubin A. E. (2013) GRO 95577 and MIL 090292: The most aqueously altered CR chondrites. *Ann. Meteorit. Soc. Meet.* #5250.

Harju E. R., Rubin A. E., Ahn I., Choi B.-G., Ziegler K. and Wasson J. T. (2014) Progressive aqueous alteration of CR carbonaceous chondrites. *Geochim. Cosmochim. Acta* **139**, 267–292.

Howard K. T., Alexander C. M. O'D., Schrader D. L. and Dyl K. A. (2015) Classification of hydrous meteorites (CR, CM, and C2 ungrouped) by phyllosilicate fraction: PSD-XRD modal mineralogy and planetesimal environments. *Geochim. Cosmochim. Acta* **149**, 206–222.

Hsu W., Guan Y., Hua X., Wang Y., Leshin L. A. and Sharp T. G. (2006) Aqueous alteration of opaque assemblages in the Ninqiang carbonaceous chondrite: Evidence from oxygen isotopes. *Earth Planet. Sci. Lett.* **243**, 107–114.

Huberty J. M., Kita N. T., Kozdon R., Heck P. R., Fournelle J. H., Spicuzza M. J., Xu H. and Valley J. W. (2010) Crystal orientation effects in $\delta^{18}O$ for magnetite and hematite by SIMS. *Chem. Geol.* **276**, 269–283.

Jilly C. E., and Huss G. R. (2012) Heterogeneous aqueous alteration in the CR2 chondrite Renazzo. *Lunar Planet. Sci. Con. XLIII,* #1348.

Jilly-Rehak C. E., Huss G. R. and Nagashima K. (2017) ^{53}Mn-^{53}Cr radiometric dating of secondary carbonates in CR chondrites: Timescales for parent body aqueous alteration. *Geochim. Cosmochim. Acta* **201**, 224–244.

Jogo K., Krot A. N., and Nagashima K. (2011) Oxygen-isotope compositions of fayalite and magnetite in CV carbonaceous chondrites Asuka-881317 and MET 00430: Implications for sources of water ice on the CV and ordinary chondrite parent asteroids. In *Workshop on Formation of the First Solids in the Solar System*. Kauai, November 7–9, 2011, LPI Contribution No. 1639, #9114.

Kallemeyn G. W., Rubin A. E. and Wasson J. T. (1994) The compositional classification of chondrites: VI. The CR carbonaceous chondrite group. *Geochim. Cosmochim. Acta* **58**, 2873–2888.

Kim S. T. and O'Neil J. R. (1997) Equilibrium and nonequilibrium O isotope effects in synthetic carbonates. *Geochim. Cosmochim. Acta* **61**, 3461–3475.

Kita N. T., Huberty J. M., Kozdon R., Beard B. L. and Valley J. W. (2011) High precision SIMS O, sulfur and iron stable isotope analyses of geological materials: accuracy, surface topography and crystal orientation. *Surf. Interface Anal.* **43**, 427–431.

Krot A. N. and Nagashima K. (2016) Evidence for oxygen-isotope exchange in chondrules and refractory inclusions during fluid-rock interaction on the CV chondrite parent body. *78th Ann. Meteorit. Soc. Meet.* #6014.

Krot A. N., Petaev M. I., Scott E. R. D., Choi B. G., Zolensky M. E. and Keil K. (1998) Progressive alteration in CV3 chondrites: More evidence for asteroidal alteration. *Meteorit. Planet. Sci.* **33**, 1065–1085.

Krot A. N., Brearley A. J., Petaev M. I., Kallemeyn G. W., Sears D. W. G., Benoit P. H., Hucheon I. D., Zolensky M. E. and Keil K. (2000) Evidence for low-temperature growth of fayalite and hedenbergite in MacAlpine Hills 88107, an ungrouped carbonaceous chondrite related to the CM-CO clan. *Meteorit. Planet. Sci.* **35**, 1365–1386.

Krot A. N., Meibom A., Weisberg M. K. and Keil K. (2002) The CR chondrite clan: Implications for early solar system processes. *Meteorit. Planet. Sci.* **37**, 1451–1490.

Krot A. N., Libourel G. and Chaussidon M. (2006) O isotope compositions of chondrules in CR chondrites. *Geochim. Cosmochim. Acta* **70**, 767–779.

Leshin L. A., Rubin A. E. and McKeegan K. D. (1997) The O isotopic composition of olivine and pyroxene from CI chondrites. *Geochim. Cosmochim. Acta* **61**, 835–845.

Lyon I. C., Saxton J. M. and Cornah S. J. (1998) Isotopic fractionation during secondary ionisation mass spectrometry: crystallographic orientation effects in magnetite. *Int. J. Mass Spectrom. Ion Processes* **172**, 115–122.

Makide K., Nagashima K., Krot A. N., Huss G. R., Hutcheon I. D. and Bischoff A. (2009) O- and magnesium-isotope compositions of calcium-aluminum-rich inclusions from CR2 carbonaceous chondrites. *Geochim. Cosmochim. Acta* **73**, 5018–5050.

Nagashima K., Krot A. N. and Huss G. (2015) Oxygen-isotope compositions of chondrule phenocrysts and matrix grains in Kakangari K-grouplet: Implication to a chondrule-matrix genetic relationship. *Geochim. Cosmochim. Acta* **151**, 49–67.

Nishiizumi K., Elmore D. and Kubik P. W. (1989) Update on terrestrial ages of Antarctic meteorites. *Earth Planet. Sci. Lett.* **93**, 299–313.

Ogliore R. C. and Jilly C. E. (2013) Gigapixel optical microscopy for meteorite characterization. *Planet. Sci.* **2**(1), 1–10.

Ogliore R. C., Huss G. R. and Nagashima K. (2011) Ratio estimation in SIMS analysis. *Nucl. Instrum. Methods Phys. Res., Sect. B* **269**, 1910–1918.

Rao C. P., Goodwin I. D. and Gibson J. A. E. (1998) Shelf, coastal and subglacial polar carbonates, east Antarctica. *Carbonates Evaporites* **13**, 174–188.

Riciputi L. R., McSween H. R., Johnson C. A. and Prinz M. (1994) Minor and trace element concentrations in carbonates of carbonaceous chondrites, and implications for the compositions of coexisting fluids. *Geochim. Cosmochim. Acta* **58**, 1343–1351.

Rowe M. W., Clayton R. N. and Mayeda T. K. (1994) O isotopes in separated components of CI and CM meteorites. *Geochim. Cosmochim. Acta* **58**, 5341–5347.

Rubin A. E., Trigo-Rodríguez J. M., Huber H. and Wasson J. T. (2007) Progressive aqueous alteration of CM carbonaceous chondrites. *Geochim. Cosmochim. Acta* **71**, 2361–2382.

Satterwhite C., and Righter K. (2012) *Antarctic Meteorite Newsletter* **35** (2).

Schrader D. L., Franchi I. A., Connolly H. C., Greenwood R. C., Lauretta D. S. and Gibson J. M. (2011) The formation and alteration of the Renazzo-like carbonaceous chondrites I: Implications of bulk-O isotopic composition. *Geochim. Cosmochim. Acta* **75**, 308–325.

Schrader D. L., Connolly H. C., Lauretta D. S., Nagashima K., Huss G. R., Davidson J. and Domanik K. J. (2013) The formation of the Renazzo-like carbonaceous chondrites II: Linking O-isotope composition and oxidation state of chondrule olivine. *Geochim. Cosmochim. Acta* **101**, 302–327.

Schrader D. L., Davidson J., Greenwood R. C., Franchi I. A. and Gibson J. M. (2014a) A water-ice rich minor body from the early Solar System: The CR chondrite parent asteroid. *Earth Planet. Sci. Lett.* **407**, 48–60.

Schrader D. L., Nagashima K., Krot A. N., Ogliore R. C. and Hellebrand E. (2014b) Variations in the O-isotope compositions of gas during the formation of chondrules from the CR chondrites. *Geochim. Cosmochim. Acta* **132**, 50–74.

Schrader D. L., Connolly, Jr., H. C., Lauretta D. S., Zega T. J., Davidson J. and Domanik K. J. (2015) The formation and alteration of the Renazzo-like carbonaceous chondrites III: Towards understanding the genesis of ferromagnesian chondrules. *Meteorit. Planet. Sci.* **50**, 15–50.

Schrader D. L., Nagashima K., Krot A. N., Ogliore R. C., Yin Q.-Z., Amelin Y., Stirling C. H. and Kaltenbach A. (2017) Distribution of ^{26}Al in the CR chondrite chondrule-forming region of the protoplanetary disk. *Geochim. Cosmochim. Acta* **201**, 275–302.

Taylor H. P. (1977) Water/rock interactions and the origin of H_2O in granitic batholiths. *J. Geol. Soc.* **133**, 509–558.

Tenner T. J., Nakashima D., Ushikubo T., Kita N. T. and Weisberg M. K. (2015) Oxygen isotope ratios of FeO-poor chondrules in CR3 chondrites: Influence of dust enrichment and H_2O during chondrule formation. *Geochim. Cosmochim. Acta* **148**, 228–250.

Tyra M. A., Farquhar J., Wing B. A., Benedix G. K., Jull A. J. T., Jackson T. and Thiemens M. H. (2007) Terrestrial alteration of carbonate in a suite of Antacrtic CM chondrites: Evidence from O and carbon isotopes. *Geochim. Cosmochim. Acta* **71**, 782–795.

Tyra M. A., Brearley A. J., and Guan Y. (2011) O isotopic compositon of secondary carbonates in CR1 chondrite GRO 95577. *Lunar Planet. Sci. Con. XLII,* #1639.

Ushikubo T., Kimura M., Kita N. T. and Valley J. W. (2012) Primordial oxygen isotope reservoirs of the solar nebula recorded in chondrules in Acfer 094 carbonaceous chondrite. *Geochim. Cosmochim. Acta* **90**, 242–264.

Velbel M. A., Long D. T. and Gooding J. L. (1991) Terrestrial weathering of Antarctic stone meteorites: Formation of Mg-carbonates on ordinary chondrites. *Geochim. Cosmochim. Acta* **55**, 67–77.

Verdier-Paoletti M., Marricchi Y., Avice G., Roskosz M., Gurenko A. and Gounelle M. (2017) Oxygen isotope constraingts on the alteration temperatures of CM chondrites. *Earth Planet. Sci. Lett.* **458**, 273–281.

Weisberg M. K. and Huber H. (2007) The GRO 95577 CR1 chondrite and hydration of the CR parent body. *Meteorit. Planet. Sci.* **42**, 1495–1503.

Weisberg M. K., Prinz M., Clayton R. N. and Mayeda T. K. (1993) The CR (Renazzo-type) carbonaceous chondrite group and its implications. *Geochim. Cosmochim. Acta* **57**, 1567–1586.

Weisberg M. K., Prinz M., Clayton R. N., Mayeda T. K., Grady M. M. and Pillinger C. T. (1995) The CR chondrite clan. *Proc. NIPR Symp. Ant. Met.* **8**, 11–32.

Weisberg M. K., McCoy T. J. and Krot A. N. (2006) Systematic and evaluation of meteorite classification. In *Meteorites and the Early Solar System II* (eds. Lauretta D. S. and McSween H. Y.), pp. 19–52.

Wilson L., Keil K., Browning L. B., Krot A. N. and Bourcier W. (1999) Earth aqueous alteration, explosive disruption, and reprocessing of asteroids. *Meteorit. Planet. Sci.* **34**, 541–557.

Young E. D., Ash R. D., England P. and Rumble D. (1999) Fluid flow in chondritic parent bodies: Deciphering the compositions of planetesimals. *Science* **286**, 1331–1335.

Young E. D. (2001) The hydrology of carbonaceous chondrite parent bodies and the evolution of planet progenitors. *Philos. Trans. R. Soc. Lond. A* **539**, 2095–2110.

Zheng Y.-F. (1991) Calculation of O isotope fractionation in metal oxides. *Geochim. Cosmochim. Acta* **55**, 2299–2307.

Zheng Y.-F. (1993) Calculation of O isotope fractionation in hydroxyl-bearing silicates. *Earth Planet. Sci. Lett.* **120**, 247–263.

Zheng Y.-F. (1995) O isotope fractionation in magnetites: structural effect and O inheritance. *Chem. Geol.* **121**, 309–316.

Zheng Y.-F. (1998) O isotope fractionation between hydroxide minerals and water. *Phys. Chem. Miner.* **25**, 213–221.

Zheng Y.-F. (1999) O isotope fractionation in carbonate and sulfate minerals. *Geochem. J.* **33**, 109–126.

Zheng Y.-F. (2011) On the theoretical calculations of O isotope fractionation factors for carbonate-water systems. *Geochem. J.* **45**, 341–354.

Zolensky M. E., Barrett R. and Browning L. (1993) Mineralogy and composition of matrix and chondrule rims in carbonaceous chondrites. *Geochim. Cosmochim. Acta* **57**, 3123–3148.

Zolensky M. E., Mittlefehldt D. W., Lipschutz M. E., Wang M.-S., Clayton R. N., Mayeda T. K., Grady M. M., Pillinger C. and Barber D. (1997) CM chondrites exhibit the complete petrologic range from type 2 to 1. *Geochim. Cosmochim Acta* **61**, 5099–5115.

Associate editor: Sara S. Russell